

marked-up manuscript version

Centennial to millennial climate variability in the far northwestern Pacific (off Kamchatka) and its linkage to the East Asian monsoon and North Atlantic from the Last Glacial Maximum to the Early Holocene

Sergey A. Gorbarenko [1], Xuefa Shi [2], Min-Te Chen [3], Galina Yu. Malakhova , [4], Aleksandr A. Bosin [1], Yanguang Liu [2], Jianjun Zou [2]



[1] V.I. Il'ichev Pacific Oceanological Institute, Russia

[2] First Institute of Oceanography, SOA, China

[3] National Taiwan Ocean University


[4] North-East Interdisciplinary Science Research Institute FEB RAS, Russia

Abstract

High resolution reconstructions based on productivity proxies and magnetic properties measured from sediment core 41-2 (off Kamchatka), reveal prevailing centennial -millennial productivity/climate variability in the northwestern (NW) Pacific from the Last Glacial Maximum (LGM) to the Early Holocene (EH). The ~~core~~-age model of core is established by AMS ¹⁴C dating using foraminifer shells ~~from the core~~ and by  correlating the productivity cycles and relative paleomagnetic intensity records with the same cycles and records ~~those~~ of  l-dated nearby core, SO-201-12KL. Our results show a pronounced feature of centennial--millennial productivity/climate cycles of in the NW Pacific ~~had~~-occurred synchronicity-synchronously with the summer East Asian Monsoon (EAM) at sub-interstadial scale during the LGM (3 cycles), Heinrich Event 1(3 cycles), ~~and~~-Bølling/Allerød warming (4 cycles), and over the EH (3 cycles). ~~Our~~Ceomparison of the


centennial-millennial NW Pacific productivity/climate cycles with the variability of the Antarctic temperature of the EPICA to the Antarctic EDML (EPICA-Dronning Maud Land (EDML)) ice core suggests a “push” effect of Southern hemisphere temperature gradients on the intensifications of the summer EAM ~~intensifications~~. Besides the linkages of NW Pacific high productivity and summer EAM, we observed that five low productivity cycles during EH are nearly synchronous with cooling in Greenland, with weakening of the summer EAM, and with decreases in solar irradiance. We propose that such centennial-millennial productivity/climate variability in the NW Pacific, associated with and sequence of sub-stadial/interstadials in the EAM from the LGM to EH, is are a persistent regional features and is quasi-synchronous, synchronous with the Greenland/North Atlantic short-term changes. We speculate that such climate synchronicity was also forced ~~also~~ by changes in Atlantic meridional overturning circulation, coupled with Intertropical Convergence Zone shifting, and reorganization of the northern westerly jets ~~reorganization~~.

1. Introduction

Model simulations and proxy-based interpretations have led to contradictory results concerning the millennial environmental variability in the northwestern (NW) Pacific and its underlying mechanisms during the last deglaciation. These model and proxy studies suggested either in-phase relationships of deglacial variability between the North (N) Atlantic and NW Pacific (Caissie et al., 2010; Chikamoto et al., 2012; Kienast and McKay, 2001; Seki et al., 2002) or out-of-phase responses (Gebhardt et al., 2008; Okazaki et al., 2010; Sarnthein et al., 2006). The in-phase relationship has been attributed to rapid atmospheric teleconnections in the N hemisphere on years-to-a decadal time scales (Max et al., 2012).  winter Arctic Oscillation, which resembles the North Atlantic Oscillation, directly influences the surface air temperature and sea level pressure over the region northwards of 35°N in East Asia. In turn, the Siberian High significantly influences

the East Asian Winter Monsoon (Wu and Wang, 2002). The out-of-phase response, however, was proposed to be driven by a seesaw mechanism, with oceanic readjustments between the Atlantic meridional overturning circulation (AMOC) and Pacific meridional overturning circulation. Recent studies on high-resolution and precisely-dated sediment cores from the subarctic NW Pacific, the Sea of Okhotsk, and the western Bering Sea show a deglacial sea surface temperature (SST) evolution similar to the northeastern (NE) Pacific and to the N Atlantic and Greenland temperature variability (Max et al., 2012). These studies suggest a close linkage to deglacial variations in AMOC associated with rapid atmospheric teleconnection, which were responsible for a quasi-synchronous SST development between the N Atlantic and N Pacific during the last deglaciation. On the basis of high resolution X-ray fluorescence (XRF) and sediment surface-color reflectance studies on western Bering Sea cores, (Riethdorf et al., (2013) further suggest a close linkage between millennial-scale productivity changes ~~to-and~~ the Dansgaard–Oeschger variability ~~were~~ registered in the North Greenland Ice Core Project (NGRIP) ice core, which had been interpreted ~~to-as~~ supporting the atmospheric coupling mechanism. A study comparing the subarctic N Pacific dust record to dust content in the NGRIP ice core also shows synchronicity of the timing of abrupt millennial changes during the last 27 ka (Serno et al., 2015). ~~Furthermore, Though~~ a recent study by Praetorius and Mix (2014), based on multidecadal-resolution foraminiferal oxygen isotope records from the Gulf of Alaska reveals a synchronicity of rapid climate shifts between the N Atlantic/Greenland (NGRIP core record) and the NE Pacific between 15.5 to 11 ka, ~~inverse relationships between the Atlantic/Pacific d~~ During the Holocene and Heinrich Event (HE) 1, ~~inverse relationships between the Atlantic/Pacific~~ are suggested in this paper while the short-term variability is either not sufficiently resolved or is decoupled.

All ~~of these the~~ instances indicate that a lack of high resolution proxy records in the NW Pacific prohibits precise assessments of any possible climatic teleconnection mechanisms across the basins. Although abrupt centennial-millennial precipitation anomalies ~~over-from~~ the Last Glacial

Maximum (LGM) to the Holocene have been reported in cave sediment $\delta^{18}\text{O}$ records of the East Asian monsoon (EAM) (Dykoski et al., 2005; Wang et al., 2001, 2005, 2008; Yuan et al., 2004), the timing and the trend of variability of Early Holocene (EH) regional climate changes are still controversial. In particular, though the EH climate has started from a strong warming in most cases, a Hani peat $\delta^{18}\text{O}$ record from northeastern China instead suggests ling events which are primarily superimposed on a Holocene long-term warming trend (Hong et al., 2009).

Here ~~we present~~ the high resolution results of a suite of productivity proxies, magnetic properties, and lithological changes from the NW Pacific sediment core LV 63-41-2 (hereafter, 41-2) (off Kamchatka) are presented and that reveal a sequence of centennial-millennial climate/productivity variability ~~over from~~ 20 ka to 8 ka. An age model of this core was constructed using Accelerator mass spectrometry (AMS) ^{14}C by AMS-14C dating and ~~then fine-tuned~~ by correlating the productivity cycles and relative paleomagnetic intensity (RPI) variability with ~~one~~ those of the well-dated nearby core, SO-201-12KL (hereafter, 12KL) (Max et al., 2012, 2014). Using ~~With our~~ methodologically robust age controls, it is possible we are able to infer a tight linkage between the centennial-millennial productivity variability in the NW Pacific and the sub-interstadial summer EAM intensifications expressed in cave sediment $\delta^{18}\text{O}$ records. ~~Our~~ These results ~~have enabled us to investigate the~~ further investigation of any mechanisms controlling the in-phase relationships of the centennial-millennial variability in the NW Pacific/EAM ~~with and~~ those underlying the Greenland/N Atlantic and Antarctic climate changes during the LGM – HE 1 – Bølling/Allerød (B/A) – Younger Dryas (YD) – EH (~20-8 ka).

2 Materials and methods

2.1 Coarse fraction measurement

Sediment core 41-2 was recovered in the NW Pacific off Kamchatka Peninsula (water depth 1924 m; 52°34' N; 160°00,6' E; core length 467 cm) during the joint Russian-Chinese expedition at R/V "Akademik M.A. Lavrentyev" in 2013. The weight percentage of the coarse fraction (CF) >63 µm and <2000 µm, sampled every 1 cm and separated by sieve washing, was calculated as ratios of CF weight to the weight of the dry bulk sediment. Semi-quantitative estimates were made of the amount of various components in the sediment CF, including terrigenous and volcanogenous particles (tephra), benthic and planktonic foraminifera, diatom frustules, and radiolarians, using a microscope to roughly estimate the proportions of different components in the sediment (Rothwell, 1989). The indicators of materials mainly transported to the study region by sea ice, such as CF and MS of sediments (Gorbarenko et al., 2003; Lisitzin, 2002; Sakamoto et al., 2005), are used as an ice rafted debris (IRD) proxy. Semi-quantitative estimates of the amount of terrigenous and volcanic particles in sediment CF allow the determination of core intervals with insignificant amounts of tephra, and therefore intervals with implications for CF and MS as an IRD index. The CF of sediments, indicator of the component of materials mainly transported to the study region by sea ice (Gorbarenko et al., 2003; Lisitzin, 2002; Sakamoto et al., 2005), is used as an ice rafted debris (IRD) proxy here. The tephra material input in the CF was estimated by semi-quantitative component analyses of this fraction with a total of 12 ranged scales. We made estimations of various components including terrigenous and volcanogenous particles, benthic and planktonic foraminifera, diatom frustules, and radiolarians in this study.

2.2 Chlorin content measurement

Chlorin content is assumed to reflect changes in primary surface ocean productivity, because continental-derived chlorophyll does not contribute to the chlorin content in deep marine sediment (Harris et al., 1996). The chlorin content of in core 41-2 was measured on samples taken every at 1

cm resolution, and at 2 cm resolution in core 12KL ~~every 2 cm~~ through the whole cores, as in Harris et al. (1996), modified using a Shimadzu UV-1650PC spectrophotometer (Zakharkov et al., 2007). ~~using a Shimadzu UV-1650PC spectrophotometer according to the modified method of Harris et al. (1996).~~

2.3 Total organic carbon (TOC), calcium carbonate and or b* measurements

Contents of TOC, CaCO₃, and biogenic opal in deep sea sediments are usually used as key parameters to assess paleoproductivity (Berger et al., 1989; Narita et al., 2002; Pahl et al., 1989; Seki et al., 2004). Shipboard color b* values correlate well with the changes in biogenic opal content in sediment cores (Nürnberg and Tiedemann, 2004) and are widely used as a paleoproductivity proxy in the NW Pacific and its marginal seas (Gorbarenko et al., 2012; Max et al., 2012; Riethdorf et al., 2013).

Total carbon content and inorganic carbon in core 41-2 were measured every 2 cm throughout the core ~~depth~~ by coulometry using an AN-7529 analyzer (Gorbarenko et al., 1998). TOC content was determined by calculating ~~computing~~ the difference between total carbon and inorganic carbon content. A color b* index (psychometric yellow–blue chromaticness) was measured with 1 cm resolution using a Minolta CM-2002 color reflectance spectrophotometer ~~that generates visible light reflectance data (400 to 700 nm wavelengths) (Harada, 2006) of the core every 1 cm. In this study we used the trend of color b* that well correlates with the changes in biogenic opal contents in sediment cores (Nürnberg and Tiedemann, 2004).~~

–

2.4 Radiocarbon dating (AMS 14C)


AMS 14C-ages were measured ~~on~~ in monospecific samples of the planktic ~~foraminifers~~ foraminifera *Neogloboquadrina pachyderma* sinistral (*N. pachyderma* sin.) from ~~a~~ the 125–250 μm

fraction, and benthic foraminifera *Epistominella pacifica*, and *Uvigerina parvocostata* from the 250–350µm fraction of the core. The radiocarbon dating ~~has been was~~ performed by ~~the~~ Dr. John Southon at the Keck Carbon Cycle AMS Facility (UCIAMS) in the Earth System Science Department of the University of California, USA. The ~~constant same~~-reservoir age (900 ± 250 yr) of the NW Pacific surface water (Max et al., 2012) was adopted in this study to ~~convert calibrate~~ the ^{14}C ages of ~~our the~~ samples into calendar ages, ~~in order to for~~ establishing consistent AMS ^{14}C chronologies of cores 41-2 and 12KL. ~~When using benthic foraminifera for AMS ^{14}C dating on our cores, we take the age difference of 1400 yrs between coexisting benthic and planktic foraminifera ages to make further corrections (Max et al., 2014).~~ All reservoir age corrected ^{14}C data were converted ~~into~~ calendar age by using Calib Rev 6.0 (Stuiver and Reimer, 1993) with the ~~IntCal09 and Marine1309 calibration curve data sets~~ (Reimer et al., 2009). When using benthic foraminifera for AMS ^{14}C dating on the cores, an age difference of 1400 yrs is taken between coexisting benthic and planktic foraminifera ages (Max et al., 2014).

2.5 Magnetic property measurements

Magnetic properties ~~analyses of cores 41-2 and 12KL~~ were measured at 2.2 cm resolution in both ~~conducted by taking samples every 2.4 cm throughout the~~ cores. ~~The V~~ volume magnetic susceptibility (MS) of these samples was measured using an AGICO MFK1-FA device. The characteristic remnant magnetization (ChRM) of the ~~cube~~ samples was measured in the same way by studying the stability of natural remanent magnetization (NRM) in the alternative magnetic fields of up to 80-100 mT on the basis of analysis of Zijderveld vector plots, using an AGICO LDA-3A device and rock-generator AGICO JR-5a (Zijderveld, 1964). The module and direction of NRM were measured on a JR-5A rock-generator after the stepwise demagnetization of reference samples by alternating magnetic fields with a vanishing amplitude (Malakhov et al., 2009). Ahysteretic remanent magnetization (ARM) was generated using an AGICO AMU-1A device and measured ~~using by~~ the JR-5A rock-generator. ~~The R~~ relative paleomagnetic intensity (RPI) of the studied core

sediments was determined by the normalization of the ChRM after demagnetization at 20 mT by ARM (ChRM/ARM) (Tauxe, 1993). The sediment paramagnetic magnetization (PM) was measured for each sample from curves of magnetic hysteresis by a J Meter coercitive spectrometer at Kazan State University, Kazan, Russia (Enkin et al., 2007; Jasonov et al., 1998).

 It relative paleomagnetic intensity (RPI) value changes in response to variability in the Earth's magnetic field present an independent chronological instrument of marine and continental sediments (Channell et al., 2009), and are widely used for sediment correlation and chronology (Kiefer et al., 2001; Riethdorf et al., 2013). PM was formed in marine sediments of silicate, paramagnetic iron sulphide (FeS), and fine clay minerals transported from land as an eolian dust through atmosphere circulation by westerly jets. Therefore, the sediment PM may serve as a proxy of the land aridity and/or atmosphere circulation pattern changes in response to climate changes. MS was mainly formed by ferromagnetic minerals delivered together with terrigenous materials from adjacent land, and is therefore related to IRD. It is the main transport agent of clastic material input into the sediment of the NW Pacific and its marginal seas (Gorbarenko et al., 2003; Lisitzin, 2002; Sakamoto et al., 2005).

2.6 XRF measurements

The Core 41-2 elemental composition of core 41-2, given in peak area (counts per second, cps), ~~were was~~ measured at 0.5 cm resolution using the Itrax XRF core scanner at the First Institute of Oceanography, State Oceanic Administration, China. The Itrax XRF core scanner was set at 20 s count times, 30 kV X-ray voltage, and an X-ray current of 20 mA. Though absolute elemental concentrations are not directly available from the micro-XRF measurements, the count values can be used as estimates of the relative concentrations. The count values may be influenced by ~~the~~ changes in the physical properties of the sediment, such as the surface roughness of the core (Röhl and Abrams, 2000). However, the grain size of the 41-2 core is rather fine and the surface has been

processed to be as flat as possible to minimize any effects from changing physical properties or roughness during the scanning.

In this study, ~~we paid~~ attention was paid to the scanning results for estimating biogenic Ba, Br and Si (Ba-bio, Br-bio and Si-bio respectively) contents in our sediment cores, which serve as proxies of productivity. The content of Ba-bio was estimated through ~~by~~ subtraction of its terrigenous component (Ba-ter) from the total bulk Ba concentration in sediment (Ba-tot). The terrigenous component, in turn, was calculated from empirical regional $(Ba/Al)_{ter}$ ratios in the sediment core with the lowest Ba-tot contents:

$$Ba\text{-}bio = Ba\text{-}tot - (Ba/Al)_{ter} * Al \text{ (by Goldberg et al. (2005))}.$$

Br-bio and Si-bio were calculated using the same technique.

Earl et al. (2016) showed that the non-destructive, high resolution X-ray Fluorescence (XRF) measurements of Ba-bio, Br-bio, and Si-bio by a core scanner or synchrotron radiation are consistent with analytically measured Ba-bio, TOC, and biogenic opal, respectively, and therefore may be used as paleoproductivity proxies (Goldberg et al., 2005; Nürnberg and Tiedemann, 2004; Riethdorf et al., 2016). Ba-bio is formed during the decay of organic matter in the water column and the uptake of Ba in settling particles (Dymond et al., 1992), and has been previously used as a paleoproxy (Goldberg and Arrhenius, 1958; McManus et al., 1998). Si-bio, related with biogenic opal in deep sea sediments, is usually used as a key parameter to assess paleoproductivity (Berger et al., 1989; Narita et al., 2002; Seki et al., 2004). Br-bio content measured using a core scanner is strongly correlated with TOC variability (Riethdorf et al., 2016) and therefore may also be used as a paleoproductivity proxy.

3. Results

AMS radiocarbon data for core 41-2 are presented in Table 1. ~~The sediment PM and MS, and~~

a suite of productivity proxies—TOC, chlorin, CaCO₃, Ba-bio, Br-bio, Si-bio contents, and color parameter b*—with four AMS ¹⁴C data. The variability of a suite of productivity proxies (color b* and contents of TOC, chlorin, CaCO₃, Ba-bio, Si-bio, and Br-bio), plus magnetic properties (RPI, sediment PM, and MS), are presented for core 41-2 versus depth (Fig. 2). We observed high productivity in the middle part of the core (at the interval ~315-230 cm), according to several productivity proxies and available AMS ¹⁴C data which could be chronologically assigned to the B/A warming right after the termination of the last glaciation (467-315 cm). The high productivity during the B/A warming is a common feature in the far NW Pacific and its marginal seas (Galbraith et al., 2007; Gorbarenko, 1996; Gorbarenko et al., 2005; Gorbarenko and Goldberg, 2005; Keigwin, 1998; Seki et al., 2004). The interval at ~230-190 cm with a decreased trend of productivity is likely associated with the YD cooling. After this low productivity/cold climate event the high productivity/warm trend in the upper 190 cm of the core is presumably related to the Holocene warming/warm-temperature condition.

Time resolutions for our core 41-2 data over LGM-YD periods are ~30 years for chlorin and color b*, ~60 years for TOC, CaCO₃ and magnetic parameters (PM, MS and RPI), and ~15 years for the Ba-bio, Br-bio, Si-bio contents. In core 41-2, the time resolutions of measured color b*, and chlorin, TOC, CaCO₃ content and magnetic parameters (PM, MS, and RPI); and Ba-bio, Br-bio, and Si-bio concentrations over the LGM-YD periods are nearly 30 years, 15 years, and 60 years respectively. The resolutions are high enough to allow us to the detection of centennial-millennial scale climate variability in the far NW Pacific. Our high-resolution productivity and magnetic records presented here. Graphical relation of the productivity proxies (chlorin, TOC, CaCO₃, Ba-bio, Br-bio, Si-bio content, and color b*) and the PM record reveal nearly-quasi-synchronous the centennial-millennial cycles likely associated with abrupt productivity/environmental variability (Fig. 2) with via mechanisms likely similar to previously established earlier regularities at the orbital-millennial scale (Fig. 2) (Broecker, 1994; Ganopolski

and Rahmstorf, 2002; Sun et al., 2012). Therefore, in particular we ~~it is suggested~~ that the sharp increases ~~shown in our productivity records demonstrates a quick the fast~~ response of the oceanic climate system of the NW Pacific environment associated with ~~to abrupt global regional~~ warming, and vice versa, similar to interstadial events in the NW Pacific and the Okhotsk and Bering Seas. The rises in temperature of surface water and environmental amelioration in the NW Pacific, the Okhotsk and Bering Seas, and the Sea of Japan are well correlated with interstadials in $\delta^{18}\text{O}$ records in the NGRIP ice core (North Greenland Ice Core Project members, 2004) and in the Chinese cave stalagmites promoting to increase productivity at the millennial scale (Gorbarenko et al., 2005; Nagashima et al., 2011; Schlung et al., 2013; Seki et al., 2002, 2004).

Each productivity proxy used here has its own specific limitations and peculiarities in its response to environmental and primary productivity changes. For example, although carbonaceous fossils (planktonic foraminifera and coccolithophorids) rain from the euphotic layer derived by primary production, and provide the main carbonate input into the sediment, CaCO_3 content in the deep sea sediment is mostly governed by climatically forced variability in the deep water chemistry and carbonate ion concentration (CO_3^{2-}), resulting in different carbonate preservation in the past (Yu et al., 2013). As for the Ba-bio proxy, Jaccard et al. (2010) suggest that in the highly productive areas, barite dissolution has been observed under suboxic conditions, precluding its application as a quantitative proxy to reconstruct past changes in export production. Although it has been suggested that biogenic opal and TOC content, being responsible for the accumulation of siliceous fossils, and siliceous plus carbonaceous fossils, respectively, present basic key proxies for the assessment of productivity changes (Berger et al., 1989), they vary in different ways at various times in sediments of the NW Pacific and its marginal seas. For example, in the Okhotsk Sea biogenic opal content lags significantly relative to TOC changes during the last deglaciation—the Late Holocene (Gorbarenko et al., 1998; Seki et al., 2004). TOC content in the hemipelagic sediment includes the organic carbon

formed by marine primary production, and the terrigenous organic material delivered from land. The input of which depends on the river runoff and sea level changes. Therefore, centennial-millennial changes in different productivity proxies vary not exactly synchronously, depending on organic matter transformation into a different proxy, and its subsequent preservation in the sediments.

The presentation of a wide range of productivity proxies allows different aspects of the transformation of primary produced organic matter into different proxies, and their preservation in sediment, to be considered. This approach provides a more reliable pattern of productivity changes. Beside productivity proxies the PM record is also used, because the sediment PM reflects the changes in the transportation of dust from continents by atmospheric circulation associated with climate change. For the statistical assessment of the centennial-millennial productivity variability, the productivity stack is calculated. It is an average of the normalized data of each proxy, given equal weight (Fig. 3).

~~In results, our productivity and magnetic records show that 6 short warm events happened during the last glacial and 4 warm events during the B/A warming (Fig. 2). During the EH, our records show 5 short cold events and 3 warm events.~~ A graphic correlation of all the applied productivity proxies with the sediment paramagnetic magnetization (PM) record shows that six short increased productivity/warmer events happened during the last glacial, and four occurred during the B/A warming (Fig. 2). During the EH five short lower productivity/colder events and three higher productivity/warmer events were found. We notice It is noted that a colder event at depth 117-122 cm with an age of ~9.12 ka (Table 1) is well-correlated with the 9.3 ka cold event in Greenland ice core records (Rasmussen et al., 2014). Moreover, a cold event identified at depth 106-109 cm of our in core 41-2 also links well with the 8.2 ka cold event in Greenland ice cores, a well-known chronostratigraphic marker in the Early to Middle Holocene boundary (Walker et al., 2012).



~~Our records of the CF percentages, amount of volcanic particles in CF, and MS indicate high~~

IRD values below a 315-cm depth of the core. A significant increase of CF to the top in the upper-220-cm of the core was mostly driven by increased tephra input (Fig. 2). Our MS record also shows higher terrigenous input in the interval of 230–205-cm included in the YD (Fig. 2). A compilation of all our 195 proxies of productivity, PM, and RPI of core 41-2 and a comparison with ones of core 12KL are shown in Fig. 3. The color b^* indices and Ca/Ti ratios (analog of CaCO_3 content) of core 12KL were extracted from Max et al. (2012, 2014) available on PANGAEA Data Publisher for Earth & Environmental Science (<http://dx.doi.org/10.1594/PANGAEA.830222>).

The share of tephra in the sediment CF shows relatively low values below 130 cm, and significantly increases in the upper part of the core (Fig. 2). Therefore, CF and MS records, controlled by the tephra share in CF, indicate high IRD inputs in the sediment of the lower part of the core, and a strong decrease towards the top in the interval 325–315 cm. MS and CF records also show some increase of IRD input in the interval 230–200 cm, related to the YD (Fig. 2).

The relative paleointensity (RPI), color b^* records, and productivity stack of core 41-2 were compared with the RPI, PM, and several productivity proxies of nearby core 12KL versus core depth (Fig. 3). The color b^* index and Ca (analog of CaCO_3 content) of core 12KL were obtained from Max et al. (2012, 2014) and PANGAEA Data Publisher for Earth and Environmental Science (<https://doi.pangaea.de/10.1594/PANGAEA.786201>). The centennial-millennial events with increased productivity shown in Fig. 2 were confirmed by the productivity stack changes for core 41-2, and correlate well with productivity events for core 12KL outlined by the productivity proxies and PM record; their correlation is also consistent with RPI variability in both cores.

4. Age model

An age model of core 41-2 was constructed using all available AMS ^{14}C dating, with more age control points identified by correlating the centennial-millennial events of the productivity proxies, RPI and PM of ~~our the studied~~ core with those of the well-dated nearby core 12KL (Max et al., 2012, 2014) (Fig. 3). The age tuning used in this study assumes a synchronous pattern of productivity, RPI and PM variability in the far NW Pacific since the last glacial, especially for closely-located cores. With this ~~conception framework~~ of age model developments, the centennial-millennial variability of productivity proxies ~~with increased productivity events, relative paleointensity (RPI) of Earth's magnetic field, and paramagnetic magnetization (PM) identified in cores 41-2 and 12KL have to be closely matched in both cores over the last glaciation—the B/A warming to the EH (Fig. 3), magnetic parameters earlier identified in core 41-2 are closely matched in the both cores; they show regionally coherent sequences of productivity/environmental cycles (events) from the last glaciation, the B/A warming to the EH (Fig. 3). We noticed~~ It was noted that the available model for core 12KL—the Tiedemann/Max age model (Max et al., 2012, 2014)—was based on the AMS ^{14}C data and correlation of color b^* index with the NGRIP $\delta^{18}\text{O}$ curve (PANGAEA Data Publisher). By adopting this age model of core 41-2, ~~all available~~ the AMS ^{14}C dating of core 12KL of Max et al. (2012, 2014) ~~(with one exception for an age dating of 16.53 ka at depth 695 cm) were~~ successfully transferred ~~successfully~~ to core 41-2 according to the correlation of related increased productivity events and RPI values within related productivity cycles and RPI values correlation (Fig. 3). The color b^* minimum in core 12KL at a depth of 706 cm, which Tiedemann and Max (PANGAEA  a Publisher) correlate with a minimum in the NGRIP $\delta^{18}\text{O}$ curve at 16.16 ka, is also clearly correlated with the color b^* minimum of core 41-2 at a depth of 348 cm (Fig. 3). All correlated AMS ^{14}C key points are also well-matched with the measured RPI curves of both cores (Fig. 3). Core 41-2 AMS ^{14}C data of 9.45 ka, 10.6 ka, 14.39 ka, and 14.61 ka at depths of 127.5 cm, 156 cm, 298 cm, and 306 cm, respectively, are fairl  close to the nearby projected ^{14}C datum from core 12 KL (Table 2), and confirm the validity of this age projection. Here

the use of the ^{14}C data of core 12KL is preferred, because this core has a higher sedimentation rate, and planktonic foraminifera for these measurements were picked from intervals with the highest Ca content, to significantly decrease a bioturbation effect.

~~Derived radiocarbon framework of both cores allow us to infer also close correlation of the productivity/environmental cycles identified in the cores with sub-interstadial of absolute U-Th dating $\delta^{18}\text{O}$ of calcite recorded in the China caves stalagmites over the 20-8 ka BP (Dykoski et al., 2005; Wang et al., 2008) (Fig. 3), which may be used for further tuning of our age model. In results, the key time points of core 41-2 were based on the available AMS ^{14}C data of core 41-2, depths correlated with core 12KL AMS ^{14}C datum plus correlation of the productivity/environmental cycles with sub-interstadials of the highly resolved, absolutely dated EAM records (Table 2). In the upper part of core we prefer to use correlation with data of core 12KL because of very high sedimentation rate and since they were measured for planktonic foraminifera.~~

5. Discussion

~~With the new age controls our productivity proxies and magnetic results of core 41-2, and some of them for core 12KL (Max et al., 2012, 2014) reveal sequence of noticeable centennial-millennial scale events of increased productivity and decreased PM in the far NW Pacific off Kamchatka over the last 21 ka (Fig. 4). As was mentioned these events changes in-phase with sub-interstadials of $\delta^{18}\text{O}$ calcite of Chinese stalagmites (CsI) associated with stronger summer EAM (Wang et al., 2008) and, to some extent, are linked to Greenland ice core sub-interstadials (GsI) (North Greenland Ice Core Project members, 2004) (Fig. 4). All the linkages suggest the centennial-millennial productivity changes in the far NW Pacific were likely associated with climatic shifts to warmer and/or higher nutrient conditions in surface water synchronously with CsI~~

of the summer EAM. Our high resolution records show clearly that three centennial-millennial warmer/higher productive (CsI/GsI) events had occurred during the LGM, three CsIs/GsIs during the HE 1, four CsIs/GsIs during the B/A warming, and three CsIs/GsIs during the EH (Fig. 4). Within the constructed age model of core 41-2, different productivity proxies and magnetic results were combined with similar data from core 12KL (Max et al., 2012, 2014). These data reveal a sequence of noticeable centennial-millennial scale productivity cycles in the far NW Pacific, which occurred in-phase with Chinese sub-interstadials (CsI) associated with a stronger summer EAM (Wang et al., 2008) over the period 21–8 ka (Fig. 4). These linkages suggest the centennial-millennial increased productivity events in the far NW Pacific were likely associated with shifts to a warmer climate and/or higher nutrient conditions in surface water synchronously with CsI of the summer EAM. High resolution records presented here show clearly that three centennial-millennial increased productivity/environment amelioration events correlated with CsI had occurred during the LGM, three CsIs during the HE 1, four CsIs during the B/A warming, and three CsIs during the EH (Fig. 4; Table 3). The possible mechanisms responsible for the in-phase relationships or the synchronicity of the centennial-millennial scale events between the NW Pacific productivity and summer EAM are discussed and proposed and discussed below.

5.1. N-S hemispheres climatic linkages of centennial-millennial climate/environment changes over the LGM - HE 1- B/A warming

Identifying any linkages of centennial-millennial climate changes in the Northern Hemisphere between the NW Pacific, EAM, and N Atlantic/Greenland and the climate changes recorded in Antarctic ice core records from the Southern Hemisphere is important to us, to deepen our understanding of the mechanisms responsible for the timing and spatial propagation patterns that resulted from the abrupt variability in the global climate and environmental system. In order to test the linkages, we demonstrate here the correlation among the highly resolved U-Th dated $\delta^{18}O$

records of the composite Hulu and Dongge caves sediments (Dykoski et al., 2005; Wang et al., 2008), the ~20-year averaged resolution $\delta^{18}\text{O}$ and Ca^{2+} content records of the GISP2 and NGRIP with 5-point running mean on the annual layer counted GICC05 age scale (Rasmussen et al., 2014), and the $\delta^{18}\text{O}$ record of the EPICA Dronning Maud Land (EDML) ice core from Antarctica (EPICA Community Members, 2006) on the methane-synchronized timescale with the NGRIP core over the past 25 ka (Fig. 5). The Ca^{2+} content in the Greenland ice cores serves as a proxy for dust content governed by atmosphere circulation changes. It has been suggested that the nearly synchronous ice core $\delta^{18}\text{O}$ and Ca^{2+} changes reflect the shifting of Greenland atmospheric dust loading and is closely linked to the atmospheric circulation and climate changes in the high latitude of N-hemisphere. Initially the persistent millennial scale changes shown in the Greenland ice core records were defined as interstadials (GI) and stadial (GS) (Johnsen et al., 1992), but have been refined by INTIMATE event stratigraphy studies which introduced the subdivision of the GI-1 into sub-interstadials GI-1a to GI-1e. Furthermore, the GS-2.1 was subdivided into sub-Stadial GS-2.1a (over the HE-1), GS-2.1b (LGM), and GS-2.1c (Björck et al., 1998; Rasmussen et al., 2014) (Fig. 5). It also has been noted that the some $\delta^{18}\text{O}$ differences in coeval $\delta^{18}\text{O}$ values between Summit and NGRIP ice cores over the LGM period, and abrupt millennial scale variations, were likely governed by changes in the N American Ice Sheet volume and N Atlantic sea ice extent, that result in the changes of meridional gradients in the $\delta^{18}\text{O}$ of Greenland ice (Seierstad et al., 2014).

On the basis of the high-resolution NGRIP core investigation (less one year) over 15–11 ka, Steffensen et al. (2008) have suggested that at the beginning of the GI, the initial northern shift of the Intertropical Convergence Zone (ITCZ), identified in a sharp decrease of dust within a 1–3 year interval, triggered an abrupt shift of Northern Hemisphere atmospheric circulation. The circulation pattern changes forced a more gradual change (over 50 years) of the Greenland air temperature associated with high latitude atmosphere circulation and westerly jets ways reorganization. Evidence from a loess grain size record in NW Chinese Loess Plateau (Sun et al., 2011), infer the linkage of

the changes in EAM strength and Greenland temperature over the past 60 ka, and suggests a common force driving both changes (Sun et al., 2011). Using a coupled climate model simulation, Sun et al. (2011) investigated the effect of a slow-down of AMOC on the monsoon system and found a stronger winter EAM that supplies more dust to the Loess Plateau with a reduction in summer monsoon precipitation over East Asia. This study indicates that AMOC is a driver of abrupt change in EAM, with the northern westerlies as the transmitting mechanism from the N Atlantic to the Asian monsoon regions. Other evidences of teleconnection between the EAM and N Atlantic on a millennial timescale come from the investigation of the Japan Sea sediments. Nagashima et al. (2011) infer that temporal changes in the provenance of eolian dust in Japan Sea sediments reflect changes in the westerly jet path over East Asia, happened in phase with Dansgaard-Oeschger cycles.

EPICA community members (2006) show that methane synchronization of the EDML and the NGRIP $\delta^{18}\text{O}$ records reveal one-to-one alignment of each Antarctic warming with a corresponding stadial in Greenland ice cores, implying a mechanism of bipolar seesaw on these time scales. Changes in the heat and freshwater flux were connected to the AMOC and a stronger AMOC leads to increased transport of heat from the Southern Ocean heat reservoir. EAM studies (Wang et al., 2001) have suggested that between 11,000 and 30,000 yr BP the Chinese interstadials (CI) recorded in $\delta^{18}\text{O}$ calcite of cave stalagmites had happened apparently synchronously with the GIs and therefore CIs were likely related to Antarctica cold events also. For example, smoothed warmer condition in the Antarctic at 23.6–24.2 ka was synchronous with abrupt climate cooling and increases in dust content in the Greenland ice cores NGRIP and GISP2, coeval to HE 2 of the N Atlantic and in phase with summer EAM weakening (GS/CS-3.1) (Fig. 5). Subsequent Antarctica cooling since 23.4 ka was accompanied by Greenland warming with two sharp interstadials GI-2.2 and GI-2.1 with nomenclature of Rasmussen et al. (2014) and China interstadial CI2 coeval with summer EAM intensification—sub interstadial CsI-2.9 (Fig. 5).—

The uncertainties in the chronologies of the Greenland and Antarctica temperature and EAM

records is very small ($<2\%$) thus suggest their tight relationship during the last 25ka (Fig. 5). Cross-correlation of the EAM intensity and Greenland climate variability calculated by correlation of $\delta^{18}\text{O}$ values between the calcite of Chinese stalagmites responsible for EAM variability (Wang et al., 2008) and NGRIP and GISP 2 ice cores responsible for the Greenland climate (Rasmussen et al., 2014) by moving windows at 1000, 2000 and 3000 years show their significant synchronization (positive correlation) during period of 16.5–9.0 ka BP (Fig. 6). The cross-correlation of the EAM and the Greenland NGRIP ice core during earlier (25–16.5 ka ago) and later (9–1 ka ago) periods demonstrates absence of significant correlation (within ranging at ± 0.25), or occurrence of weak synchronization (positive correlation) (Fig. 6). The statistics imply that the seesaw mechanism between the EAM/NW Pacific and the Greenland/N Atlantic during 25–1 ka is not effective, however being in line with empiric results of the EAM and the Greenland teleconnection by shifting of the westerly jet path (Nagashima et al., 2011; Sun et al., 2011).

It also has been suggested that a monsoon intensity index including the EAM was controlled not only by Northern Hemisphere temperature ('pull' on the monsoon, which is more intense during boreal warm periods), but also by the pole to equator temperature gradient in the Southern Hemisphere ('push' on the monsoon which is more intense during cold periods) that leads to enhanced boreal summer monsoon intensity and its northward propagation (Rohling et al., 2009; Rossignol-Strick, 1985; Xue et al., 2004). Since the summer EAM transports heat and moisture from the West Pacific Warm Pool (WPWP) across the equator and to higher northern latitudes (Wang et al., 2001), the temperature gradient in the Southern Hemisphere "pushes" the summer EAM intensity by means of its influence on the latitudinal/longitudinal migrations or expansion/contraction of the WPWP. This also explains the different form of responses of EAM and Greenland interstadials and sub-interstadials, because the migration of the WPWP may have responded much more slowly than the atmosphere. All the above interpretations are consistent with observed here, that the variability in the $\delta^{18}\text{O}$ record of Chinese EAM changes was more gradual

then in the $\delta^{18}\text{O}$ of Greenland ice cores, and the amplitude changes of the EAM are more similar to the Antarctic air temperature changes (Fig. 5).

With the same subdivision as in Greenland records, the EAM sub-interstadials (CsI)/NW Pacific centennial-millennial productivity/environment cycles were put on the N-S hemispheres climate variability with three CsIs identified from the interval of 25–20 ka (Fig. 5). Moreover, we found three EAM/NW Pacific sub-interstadials within GS-2.1a (namely CsI 2.1, CsI 2.2 and CsI 2.3), four CsIs in GS-2.1b (CsI 2.4 to CsI 2.7), and two in GS-2.1c (CsI 2.8 and CsI 2.9) (Fig. 5). During B/A warming when Antarctic temperature was decreased, four EAM sub-interstadials (CsI 1a–CsI 1e) have varied in phase with Greenland sub-interstadials (Björck et al., 1998).

Our results derived from two studied cores indicate tight in-phase linkages between the far NW Pacific centennial-millennial productivity/environment cycles and the summer EAM intensity sub-interstadials variability (Fig. 4) over GS-2.1–GI-1. These evidence leads us to suggest that the centennial-millennial changes in the NW Pacific and EAM have been forced by similar/or may be less pronounced mechanisms as for interstadials by the shifting of the ITCZ with reorganization of the N Hemisphere atmospheric circulation and the northern westerly jets. Though the responses of the EAM sub-interstadials are more smoothly compared with Greenland ones (Fig. 5), the most of them had occurred synchronicity with ones of the Greenland NGRIP ice core and out-of phase with ones of the Antarctica record (Fig. 5). Thus we infer that revealed for studied cores centennial-millennial productivity/environment cycles over 20–8 ka ago are persistent peculiarities of the productivity/environment variability of the NW Pacific couples with EAM sub-interstadials changes which may be used as template in the regional high-resolution paleoceanography and sediment stratigraphy. Four productivity/environment events in the far NW Pacific during the B/A warming had occurred in-phase with the EAM and Greenland temperature sub-interstadials (Figs. 4 and 5). Recent high-resolution investigations on Bering Sea sediment cores from the “Bering Green Belt” (Kuehn et al., 2014) have documented four well-dated laminated sediment layers during the

~~B/A warming beginning of Holocene, with one from them for the Preboreal. The synchronicity of Bering Sea laminated sediment layers with the Greenland sub-interstadial during B/A warming provides one more piece of evidence supporting the close atmospheric teleconnection between the N Pacific, the EAM, and the N Atlantic.~~

The identification of any linkages between centennial-millennial climate changes in the Northern Hemisphere (NW Pacific, EAM, and N Atlantic/Greenland) and the climate changes recorded in Antarctic ice cores representative of the Southern Hemisphere is important for deepening understanding of the mechanisms responsible for the timing and spatial propagation patterns that resulted from abrupt variability in the global climate and environmental system. In order to test these linkages, the centennial-millennial productivity/climate events in the NW Pacific outlined by the productivity stack are correlated with a variety of other records. These are: the highly resolved U-Th dated $\delta^{18}\text{O}$ records of the composite Hulu and Dongge stalagmites (Dykoski et al., 2005; Wang et al., 2008); the ~20-year averaged resolution $\delta^{18}\text{O}$ and Ca^{2+} content records of the GISP2 and NGRIP, with a five-point running mean on the annual-layer counted GICC05 age scale (Rasmussen et al., 2014); the $\delta^{18}\text{O}$ record of the EPICA Dronning Maud Land (EDML) ice core from Antarctica (EPICA Community Members, 2006) on the methane synchronized timescale with the NGRIP core; and the Siberian climate calculated from pollen records of the Lake Baikal region (Bezrukova et al., 2011) over the past 25 ka (Fig. 5). The Ca^{2+} content in the Greenland ice cores serves as a proxy for dust mobilization on the land, and for transfer in the high latitudes of the N Hemisphere by an atmosphere governed by climate and atmospheric circulation changes (Sun et al., 2012). It has been suggested that the nearly synchronous ice core $\delta^{18}\text{O}$, and Ca^{2+} millennial-scale changes reflect the shifting of the Greenland atmospheric dust loading, which is closely linked with the atmospheric circulation and climate changes in the high latitudes of the N Hemisphere, where the EAM plays an important role (Ruth et al., 2007). Initially, the persistent millennial-scale changes shown in the Greenland ice core records were defined as interstadials (GI) and stadials (GS)

(Johnsen et al., 1992), but have been refined by INTIMATE stratigraphy studies which introduced the subdivision of the GI-1 into sub-interstadials GI-1a to GI-1e. Furthermore, the GS-2.1 was subdivided into sub-stadials GS-2.1a (over the HE 1), GS-2.1b (LGM), and GS-2.1c (Björck et al., 1998; Rasmussen et al., 2014) (Fig. 5).

During the construction of the age model, a strong correlation was established between the centennial-millennial productivity/environment events in the NW Pacific cores, and the sub-interstadials of the summer EAM over the LGM-HE 1-B/A (Fig. 5), suggesting a strong, causal teleconnection. This suggests that, in addition to the six centennial-millennial productivity/environment cycles over the LGM-HE 1 established in the NW Pacific cores, another three abrupt events likely took place in the NW Pacific coeval with CsIs outlined by the $\delta^{18}\text{O}$ of Chinese stalagmites over the interval 25–20 ka (Fig. 5). Therefore, it was found that three EAM/NW Pacific sub-interstadials occurred within GS-2.1a (namely CsI-GS2.1-1, CsI-GS2.1-2, and CsI-GS2.1-3), four CsIs occurred within GS-2.1b (CsI-GS2.1-4 to CsI-GS2.1-7), and two occurred within GS-2.1c (CsI-GS2.1-8 and CsI-GS2.1-9) (Fig. 5).

It also has been noted that there are some $\delta^{18}\text{O}$ differences between coeval $\delta^{18}\text{O}$ values in the Summit and NGRIP ice cores over the LGM-HE 1 period, which were likely governed by changes in the N American Ice Sheet volume and N Atlantic sea-ice extent, resulting in changes of the meridional gradients in the $\delta^{18}\text{O}$ of Greenland ice (Seierstad et al., 2014). Such differences in the Summit/NGRIP $\delta^{18}\text{O}$ values may explain why the correlation of the EAM/NW Pacific sub-interstadials with the Greenland sub-interstadials recorded in the $\delta^{18}\text{O}$ and Ca^{2+} records of the GISP2 and NGRIP cores was more clear during LGM, and less pronounced over the HE 1 (GS-2.1a) (Fig. 5).

On the basis of the high-resolution NGRIP core investigation (less than one year) over 15–11 ka, Steffensen et al. (2008) have suggested that at the beginning of the GI, the initial northern shift

of the Intertropical Convergence Zone (ITCZ), identified from a sharp decrease of dust within a 1–3 year interval, triggered an abrupt shift in Northern Hemisphere atmospheric circulation. Such circulation pattern changes forced a more gradual change (over 50 years) of the Greenland air temperature, associated with the reorganization of high latitude atmospheric circulation and westerly jets. Evidence from a loess grain size record in the NW Chinese Loess Plateau (Sun et al., 2012), implies a link between the changes in EAM strength and the Greenland air temperatures over the past 60 ka, and suggests that a common force was driving both changes (Sun et al., 2012). Using a coupled climate model simulation Sun et al. (2011) investigated the effect of a slow-down of AMOC on the monsoon system, and found that a stronger winter EAM, accompanied with a reduction in summer monsoon precipitation over East Asia, supplies more dust to the Chinese Loess Plateau and likely also to the NW Pacific. This study indicates that the AMOC is a driver of abrupt change in the EAM system, with the northern westerlies as the transmitting mechanism from the N Atlantic to the Asian monsoon regions. Other evidence of teleconnections between the EAM and N Atlantic on a millennial timescale come from the investigation of sediment cores from the Sea of Japan. Nagashima et al. (2011) infer that temporal changes in the provenance of eolian dust in sediments from the Sea of Japan reflect changes in the westerly jet path over East Asia, which happened in-phase with the Dansgaard-Oeschger cycle.

EPICA community members (2006) show that methane synchronization of the EDML and the NGRIP $\delta^{18}\text{O}$ records reveal one-to-one alignment of each Antarctic warming with a corresponding stadial in the Greenland ice cores, implying a bipolar seesaw mechanism on these time scales. Changes in the heat and freshwater flux were connected to the AMOC, and a stronger AMOC leads to the increased transport of heat from the Southern Ocean heat reservoir. As a result of EAM investigations Wang et al. (2001) have suggested that between 11,000 and 30,000 yr BP the Chinese interstadials (CI) recorded in $\delta^{18}\text{O}$ calcite of cave stalagmites had happened apparently

synchronously with the GIs. Therefore, CIs were also likely related to Antarctic cold events. In confirmation, smoothed warmer conditions in the Antarctic at 23.6–24.3 ka were synchronous with abrupt climate cooling and increases in dust content in the Greenland ice cores NGRIP and GISP2, coeval to HE 2 of the N Atlantic, and in-phase with the weakening of the summer EAM (GS/CS-3.1) (Fig. 5). The Antarctic cooling since 23.4 ka was accompanied by warming in Greenland, with two sharp interstadials GI-2.2 and GI-2.1 (Rasmussen et al., 2014) and China interstadial CI-2 coeval with sub-interstadial CsI-GS2.1-9 associated with summer EAM intensification (Fig. 5). Over the LGM period, most of the sub-interstadials in the NW Pacific/summer EAM had occurred during abrupt Antarctic temperature decreases, while during HE 1 sub-interstadial linkages between the N and S hemispheres are less evident (Fig. 5).

It has also been suggested that a monsoon intensity index including the EAM was controlled not only by Northern Hemisphere temperature (“pull” on the monsoon, which is more intense during boreal warm periods), but also by the pole-to-equator temperature gradient in the Southern Hemisphere (“push” on the monsoon, which is more intense during the boreal cold periods) that leads to enhanced boreal summer monsoon intensity and its northward propagation (Rohling et al., 2009; Rossignol-Strick, 1985; Xue et al., 2004). Since the summer EAM transports heat and moisture from the West Pacific Warm Pool (WPWP) across the equator and to higher northern latitudes (Wang et al., 2001), the temperature gradient in the Southern Hemisphere “pushes” the summer EAM intensity by means of its influence on the latitudinal/longitudinal migrations or expansion/contraction of the WPWP. This also explains the difference in responses of the EAM and Greenland interstadials and sub-interstadials, because the migration of the WPWP may have occurred more slowly than the atmospheric changes. The changes in the $\delta^{18}\text{O}$ of Chinese cave stalagmites were more gradual than in the $\delta^{18}\text{O}$ of Greenland ice cores, and were more similar to the Antarctic air temperature changes (Fig. 5)



During B/A warming when Antarctic temperatures decreased, four EAM sub-interstadials (CsI-GI1-a to CsI-GI1-e), coeval with established NW Pacific centennial-millennial productivity/environment cycles, also varied in-phase with Greenland sub-interstadials (Björck et al., 1998) (Fig. 5). Recent high resolution investigations of Bering Sea sediment cores from the “Bering Green Belt” (Kuehn et al., 2014) have documented four well-dated laminated sediment layers during the B/A warming-beginning of the Holocene, with three of them within the B/A. The synchronicity of the Bering Sea laminated sediment layers with the Greenland sub-interstadial during B/A warming provides one more piece of evidence supporting the close atmospheric teleconnection between the N Pacific, EAM, and N Atlantic.

The strongly in-phase linkages between the NW Pacific centennial-millennial productivity/environment cycles, and the sub-interstadials of summer EAM intensity over GS-2.1–GI-1 (Figs. 4 and 5) suggest that these abrupt changes in the NW Pacific and EAM have been forced by similar, or less pronounced, mechanisms to interstadials, such as the shifting of the ITCZ with the reorganization of atmospheric circulation and the northern westerly jets. In-phase teleconnection of the NWP/EAM sub-interstadials with those in Greenland was also observed during LGM-B/A warming. This was weaker during HE 1, which is probably related to differences in $\delta^{18}\text{O}$ between the GISP 2 and NRGIP.

–

5.2 NW Pacific productivity trends over the LGM–HE 1–

5.2 The EH

–

During the EH the records presented here show a series of abrupt increasing/decreasing productivity events in the NW Pacific, correlated with sub-interstadials (CsI-EH-1, CsI-EH-2, CsI-EH-3)/sub-stadials (CsS-EH-1, CsS-EH-2, CsS-EH-3, CsS-EH-4, CsS-EH-5) of the $\delta^{18}\text{O}$

records of the Dongge and Hulu caves (Dykoski et al., 2005; Wang et al., 2008) and Greenland ice cores (North Greenland Ice Core Project members, 2004) (Figs. 4 and 5; Table 3). A visual comparison with the EAM and Greenland ice core records show synchronicity (positive correlation) of the increased productivity centennial events in the NW Pacific with the abrupt warmer climate cycles in Greenland and the summer EAM intensity events, and vice versa over the EH as well (Figs. 4 and 5). The dated pollen reconstructed the vegetation/climate variability of south Siberia (Lake Baikal region) (Bezrukova et al., 2011) demonstrated nearly the same type of centennial-millennial climate variability—confirming their common patterns of change in the N Hemisphere (N Atlantic, NW Pacific, EAM) over the EH (Fig. 5). Well-dated, high resolution lithological and geochemical results from the Yanchi playa (NE China) also clearly show a separation of three sharp cooling events at 8.2 ka, 9.9–10.1 ka, and 11.0–11.2 ka, synchronous with the cooling shown in the Greenland ice core records (Yu et al., 2006). Yu et al. (2006) explain this correlation through linkages of the tropical Pacific and the N Atlantic. Moreover, high resolution geochemical and lithological analyses of the Arolik Lake sediments (southwestern Alaska) provide evidence that centennial-scale climate shifts during the Holocene were similar in the sub-polar regions of the N Atlantic and N Pacific (Hu et al., 2003).

These regional climate shifts also occurred concurrently with the periodicities of solar activity and the production of the cosmogenic nuclides ^{14}C and ^{10}Be . The production rates of these cosmogenic nuclides are negatively correlated with total solar irradiance due to the strength of magnetic fields embedded into the solar wind. Small variations in solar irradiance could be responsible for pronounced changes in northern high-latitude climate and environments (Hu et al., 2003). The variability of sub-polar N Atlantic ice drifting, recorded in the percentage of hematite-stained grains in the sediment core (Bond et al., 2001), though having lower time resolution and dating precision compared with production of the cosmogenic nuclides, is consistent

with other centennial climate changes in the N Hemisphere during EH within a timing precision of 200 years.

Quasi-synchronicity of the changes in the centennial-millennial productivity and magnetic proxies obtained in the two studied cores, with the sub-interstadials in $\delta^{18}\text{O}$ records of Chinese cave speleothem, the Greenland ice cores, and with the nuclide ^{14}C production during the EH (Figs. 4, 5), imply that the variability of the NW Pacific climate and environmental conditions has been strongly related to the EAM and N Atlantic/Greenland climate changes through atmospheric coupling mechanisms over the studied period of 20–8 ka. In summary, the NW Pacific results presented here indicate a tight linkage and coherent, persistent pattern of centennial-millennial scale climate changes in the N Hemisphere over the LGM-EH, which may serve as a template in high resolution paleoceanography and sediment stratigraphy of the moderate-high latitudes of the N Pacific.

Since whether N Atlantic-N Pacific climate and hydrological linkages are in-phase or out-of-phase teleconnections is still debated, empirical data obtained from sediment cores off Kamchatka allow the provision of an additional test for clarifying this problem at a high resolution. Previously, it was stated that the N Pacific centennial-millennial productivity/climate changes are strongly associated with the EAM system variability, which may serve as key records for the N Pacific due to being the most reliable chronology of the East Asia-N Pacific region. $\delta^{18}\text{O}$ records of the GISP2 and NGRIP on the GICC05 age scale (Rasmussen et al., 2014) may serve as key records for the N Atlantic. The uncertainty in the chronologies of the Greenland and EAM records is very small (<2%) thus suggesting statistical estimation of their correlation during the last 25 ka.

Cross correlation (CC) between $\delta^{18}\text{O}$ values of Chinese stalagmites (Wang et al., 2008)—responsible for EAM/Pacific variability—and NGRIP and GISP2 ice cores (Rasmussen et al., 2014)—responsible for the Greenland/N Atlantic changes—using moving windows at 1000, 2000, and 3000 years shows their more significant synchronization (from -0.6 to -0.9) during the

period 16.5–8.5 ka (Fig. 6). During earlier (25–16.5 ka) and later (8.5–1 ka) periods there are differences in CC between the EAM-NGRIP and the EAM-GISP2. However, both CC during these periods show the occurrence of weak synchronization and/or the absence of significant correlation (within a range of ± 0.25) (Fig. 6). Significant synchronization was also indicated by CC between EAM-NGRIP during the Middle–Late Holocene. More discrepancies in both CCs were observed over 19.5–16.5 ka, which may be explained by errors in age measurements and/or by differences in atmospheric teleconnection between the EAM and the GISP2/NGRIP cores due to their different locations in Greenland. The statistics imply that the seesaw mechanism between the EAM/NW Pacific and the Greenland/N Atlantic during 25–1 ka is not effective. However, they are in line with empirical data of the EAM/N Pacific and the Greenland/N Atlantic teleconnection by shifting of the westerly jet path (Nagashima et al., 2011; Sun et al., 2012).

Beside of the centennial–millennial productivity/environmental cycles, we find common NW Pacific productivity trends over the LGM and Heinrich E 1 with some differences in other types of productivity proxies. According to the sharp increase of Antarctica temperature, dust content in the Greenland ice cores and significant decrease in the summer EAM we put boundary of LGM/HE 1 on nearly the 17.8 ka ago (Fig. 5). This age is a little earlier to that being placed at ~ 17.5 ka which is a timing for the beginning of catastrophic iceberg discharges in the HE 1, but nearly coincides with the abrupt increase of the $^{231}\text{Pa}/^{230}\text{Th}$ ratio in the N Atlantic core OCE326-GGC5, which marks the beginning of the collapse of AMOC (McManus et al., 2004).

During the LGM most productivity proxies demonstrate minimum primary production in the far NW Pacific without definite trends although the Si bio of core 41-2 and color b^* of core 12KL show even small negative trend versus time (Fig. 4). Severe environmental condition in the central Asia inferred from vegetation reconstruction (Bezrukova et al., 2011) (Fig. 5) promote to increase in cold season sea ice covering and high IRD accumulation in studied region (Fig. 4) that hamper

productivity. It is consistent with early established minimum of productivity in the NW Pacific due to strong stratification prevented nutrients supply for supporting productivity in surface waters (Gebhardt et al., 2008).—

Since 17.8 up to 15.5 ka, the core 41-2 productivity proxies such as Ba-bio, Br-bio, TOC and chlorin, associated with production of calcareous phytoplankton (mostly coccolithophores), show significant increased trends simultaneous to gradual Antarctic warming accompanied by strongly diminished of AMOC (McManus et al., 2004). The patterns are consistent with the see-saw N-S hemispheres mechanism (Broecker, 1998). The diminished AMOC resulted in a major cooling of the N Atlantic surface water and, most likely, reduced water evaporation in the N Atlantic and therefore Atlantic-Pacific moisture transport. This condition facilitates a reduction of precipitation and hence an overall increase of surface water salinity and decrease of surface stratification in the N Pacific. Moreover, this condition promotes an intensification of the intermediate water ventilation in the N Pacific and also nutrient supply into euphotic layer. The observed trends of our productivity proxies are in concord with strong intensification of the intermediate depth water ventilation in the N Pacific during HE 1 (Max et al., 2014) based on the $\delta^{13}\text{C}$ foraminifera data from the intermediate water and radiocarbon derived ventilation ages. However, rather constant CaCO_3 values in both cores (water depth 1924-2145 m) during LGM-HE 1 do not indicate the changes of the water ventilation at these depths in the N Pacific over that time span because carbonate concentration in the sediment strongly defined by the ventilation (Yu et al., 2014). While the productivity proxies Si-bio and color b^* , associated with siliceous phytoplankton production (mostly diatoms), do not show significant trends since HE 1 to ~15.5 ka. The strong sea ice effect indicated by our CF and MS records (Figs. 2; 4) was more significant in our studied area and likely overwhelm the productions of diatom algae for coccolithophores due to a large spring-early summer surface water stratification during seasonal sea ice melting.—

A sharp increase of NW Pacific primary production since ~15.5 ka was indicated by most

our productivity proxies which culminated by strong productivity peak of sub-interstadial GI-1e at beginning of the B/A warming (Fig. 4). Synchronous decrease of sea ice influence in the studied region since ~15.5 ka marked by dropping in the CF and MS was favor for decrease of surface stratification the rise of diatom production as indicated by the sharp increases of Si-bio and color b* (Figs. 4 and 2). The timing of decrease in the sea ice cover since ~15.5 ka is consistent with the surface ocean warming (Max et al., 2012) and also consistent with the central Asia vegetation/environment amelioration inferred by Bezrukova et al. (2011) by pollen reconstructions (Fig. 5). Such pattern of the productivity changes in the N Pacific and the Bering Sea during glacial/interglacial transition was observed in other cores (Caissie et al., 2010; Galbraith et al., 2007; Gebhardt et al., 2008; Keigwin, 1998) and was, likely, a persistent feature for the N Pacific and its realm forced by resumption of the AMOC at the B/A beginning coeval with the cooling in the Antarctica (Fig. 5). In the Okhotsk Sea, being strongly intruded in the NE Asia continent, the beginning of the diatom production and accumulation of the diatomaceous sediments had occurred only since the Middle Holocene (5–6 ka BP) due to the later diminish of sea ice cover and later breakdown of spring/early summer surface water stratification compared with ones of the far NW Pacific (Gorbarenko et al., 2014).

–

5.3 The EH

–5.3 NW Pacific productivity trends over the LGM-HE 1

Besides the centennial-millennial productivity/environmental cycles, common NW Pacific productivity trends are found over the LGM and HE 1 with some differences in other types of productivity proxies. According to the sharp increase in Antarctic temperature, dust content in the Greenland ice cores, and significant decrease in the summer EAM, a boundary of LGM/HE 1 was defined at around 17.8 ka (Fig. 5). This is a little earlier than ~17.5 ka, which marks the beginning of catastrophic iceberg discharges in the HE 1, but nearly coincides with the abrupt increase of the

$^{231}\text{Pa}/^{230}\text{Th}$ ratio in the N Atlantic core OCE326-GGC5, which marks the beginning of the collapse of AMOC (McManus et al., 2004).

During the LGM, most of the productivity proxies demonstrate minimum primary production in the far NW Pacific without definite trends, although the color b^* of core 12KL shows a small negative trend (Fig. 4). Severe environmental conditions in central Asia, inferred from vegetation reconstruction (Bezrukova et al., 2011) (Fig. 5), promoted an increase in winter sea ice covering consistent with high IRD accumulation in the studied region, inferred from CF and MS records (Fig. 4), that hamper productivity. It is in concord with the established minimum of productivity in the NW Pacific due to strong stratification preventing the supply of nutrients required to support productivity in surface waters (Gebhardt et al., 2008).

From 17.8 to 15.3 ka, some productivity proxies of core 41-2—namely TOC and chlorin associated with the production of calcareous phytoplankton (mostly coccolithophores)—show significantly increased trends simultaneously to gradual Antarctic warming, accompanied by a strongly diminishing AMOC (McManus et al., 2004). The diminished AMOC resulted in a major cooling of the N Atlantic surface water and, most likely, reduced water evaporation in the N Atlantic and therefore Atlantic-Pacific moisture transport. This condition facilitates a reduction of precipitation and hence an overall increase of surface water salinity, and decrease of surface stratification in the N Pacific. This condition promotes an intensification of the intermediate water ventilation in the N Pacific, and therefore the nutrient supply into the euphotic layer. The observed trends of productivity proxies are in concord with strong intensification of the intermediate-depth water ventilation in the N Pacific during HE 1 (Max et al., 2014), based on the $\delta^{13}\text{C}$ foraminifera data from the intermediate water and radiocarbon-derived ventilation ages. However, fairly constant CaCO_3 values in both cores (water depth 1924–2145 m) during LGM-HE 1 do not indicate that the water ventilation penetrated to deep water in the N Pacific over that time span, because carbonate concentration in the sediment is strongly defined by the ventilation of bathed water (Yu et al., 2014).

While the productivity proxies Si-bio and color b*, associated with siliceous phytoplankton production (mostly diatoms), do not show significant trends during HE 1 up to ~15.3 ka, the strong sea ice effect with high IRD input up to 15.3 ka, shown by CF and MS records, (Figs. 2 and 4) was significant in the studied area and probably overwhelmed the production of diatom algae for coccolithophores, due to a large spring–early summer surface water stratification during seasonal sea ice melting.

A sharp increase in NW Pacific primary production, and a rise in diatom production since ~15.3 ka, indicated by most productivity proxies and Si-bio and color b* records with a culmination at sub-interstadial GI1-e of B/A warming, was likely induced by a decrease in sea ice influence and its spring melting, favoring a weakening of surface stratification (Figs. 4 and 2). The timing of the decrease in the sea ice cover since ~15.3 ka is consistent with the surface water warming (Max et al., 2012), and with the central Asian vegetation/environment amelioration inferred by Bezrukova et al. (2011) from pollen reconstructions (Fig. 5). Such a pattern of productivity changes in the N Pacific and the Bering Sea during glacial/interglacial transitions has been observed in other cores (Caissie et al., 2010; Galbraith et al., 2007; Gebhardt et al., 2008; Keigwin, 1998) and was likely a persistent feature for the N Pacific and its realm, forced by the resumption of the AMOC at the B/A warming coeval with the cooling in Antarctica (Fig. 5). In the Okhotsk Sea, the beginning of the diatom production and accumulation of the diatomaceous sediments had begun only in the Middle Holocene (5–6 kyr BP) due to the later reduction of sea-ice cover, and later breakdown of spring/early summer surface water stratification (Gorbarenko et al., 2014).

During EH our records demonstrate a series of abrupt cold Chinese sub-stadials (CsS) and warm CsIs that are well correlated with variability shown in Dongge and Hulu caves $\delta^{18}\text{O}$ records (Dykoski et al., 2005; Wang et al., 2008), and $\delta^{18}\text{O}$ records of Greenland ice cores: CsS1 (~8.2ka), CsS2 (~9.2ka), CsI1, CsS3 (~10.2ka), CsI2, CsS4 (~10.9ka), CsS4' (~11.1ka), and CsI3 (Fig. 4). These sub-stadials and sub-interstadial were also put on the N-S hemisphere climate variability

patterns (Fig. 5). Visual comparison with the EAM and Greenland ice cores records show synchronicity (positive correlation) of the warmer climate/increased productivity events in the NW Pacific with the Greenland abrupt warmer climate cycles and summer EAM intensity events and vice versa over the EH as well (Figs. 4 and 5). Pollen reconstructed dated variability of the climate/environment conditions of the southeastern Siberia (Lake Kotokel, Lake Baikal region) (Bezrukova et al., 2011) demonstrated nearly the same type of the centennial-millennial climate variability patterns that shows positive climate linkages with climate in the North Hemisphere (N Atlantic, NW Pacific, EAM) over the EH (Fig. 5). Well-dated high resolution lithological and geochemical results from the Yanchi playa (NE China) clearly show a separation of three sharp cooling events at 8.2 ka, 9.9–10.1ka, and 11.0–11.2 ka, synchronous with the cooling shown in the Greenland ice core records (Yu et al., 2006). Yu et al. (2006) explain that correlation by linkages of the tropical Pacific and the N Atlantic. Moreover, high resolution geochemical and lithological analyses of the Arolik Lake sediments (southwestern Alaska) provide evidence that centennial-scale climate shifts during the Holocene were similar between the subpolar regions of the N Atlantic and N Pacific (Hu et al., 2003).

These regional climate shifts had occurred coherent with the periodicities of solar activity and production of the cosmogenic nuclides ^{14}C and ^{10}Be . The production rates of these cosmogenic nuclides are negatively correlated with total solar irradiance through the strength of magnetic fields embedded into solar winds speed. Small variations in solar irradiance could be responsible for pronounced changes in northern high latitude environments (Hu et al., 2003). Our records of the centennial-millennial warmer climate/increased productivity cycles in the far NW Pacific are simultaneous with the sharp variability in the EAM and the Greenland temperature over the EH and in phase, within the uncertainty of our age controls, with the decreased production of nuclide ^{14}C and therefore with increased solar input and vice versa (Fig. 5). Nearly synchronicity in the changes of the centennial-millennial productivity and magnetic proxies obtained in the two studied cores

~~with the $\delta^{18}\text{O}$ records of Chinese cave sediments, the Greenland ice cores, and with the nuclide ^{14}C production during the EH (Figs. 4, 5) imply that variability of the NW Pacific climate and environmental condition has been tightly related with EAM and N Atlantic/Greenland climate changes by atmospheric coupling mechanisms over the studied period of 20–8 ka. In summary, our analysis indicates a tight linkage and coherent, persistent pattern of the centennial–millennial scale climate changes in the N Hemisphere over the LGM–EH which may be serve as template in high-resolution climate variabilities and sediment stratigraphy of the moderate–high latitudes.—~~

6. Conclusion

This study presents high resolution records of a suite of productivity proxies (TOC, CaCO_3 , chlorin, color b^* , Ba-bio, Br-bio, Si-bio), ~~and content of sediment lithological (CF), and magnetic properties (MS, PM and RPI)~~ from a sediment core 41-2, taken from the NW Pacific (East Kamchatka slope). ~~Our r~~Results presented here reveal indicate a sequence of 13 centennial-millennial scale regional productivity increased /environment amelioration events over the LGM–EH (20–8 ka) in the far NW Pacific.

The age model of core 41-2 was constructed by using available AMS ^{14}C dating, with more age control points identified by correlating the centennial-millennial productivity events of the productivity proxies, RPI and PM of ~~our the~~ core with those of the well-dated nearby core 12KL (Max et al., 2012, 2014). Thus, all available AMS ^{14}C dating of core 12KL (~~with one exception for an age dating of 16.53 ka at depth 695 cm~~) were transferred was projected successfully to core 41-2. Based on putting all radiocarbon data of both cores on the $\delta^{18}\text{O}$ record of the Chinese cave stalagmites (Wang et al., 2008), the close time correlation of NW Pacific productivity events with sub-interstadials in the summer EAM over the period 20–8 ka was inferred and used for further fine age model construction. Three NW Pacific abrupt productivity increase events are strongly linked to

CsIs during the LGM (20–17.8 ka); three during HE 1 (17.8–14.7 ka), four during B/A warming, and three over the EH.

~~Derived radiocarbon framework of both cores allow us to infer also close correlation of the productivity/environmental cycles identified in these cores with sub-interstadial of absolute U-Th dating $\delta^{18}\text{O}$ of calcite recorded in the China caves stalagmites over the 20–8 ka BP (Dykoski et al., 2005; Wang et al., 2008), which were used for further fine age model construction. Therefore our records from studied cores show synchronicity of NW Pacific centennial-millennial higher productivity/environment amelioration events with EAM sub-interstadials during 20–8 ka. Three NW Pacific abrupt productivity increase events are tightly linked to CsIs during the LGM (20–17.8 ka), three during HE 1 (17.8–14.7 ka), and four during B/A warming and three over the EH.~~

~~Our new The reconstruction in this paper suggests that the NW Pacific centennial-millennial productivity increase and the summer EAM intensified-intensification events are positively correlated with Greenland abrupt warmings, indicating a tight-strong atmospheric teleconnection between the N Pacific and the N Atlantic, most likely by ITCZ shifting and reorganization of the northern westerlies. and This echoes the similar mechanism proposed in previous studies for the N hemisphere interstadials and stadials (Caissie et al., 2010; Kienast and McKay, 2001; Max et al., 2012; Riethdorf et al., 2013). Especially highlighted here is that our comparison of the NW Pacific centennial-millennial productivity events/EAM sub-interstadial with ~~to~~ $\delta^{18}\text{O}$ records of the EDML ice core and of the Chinese stalagmites on the centennial-millennial time scale over glaciation and deglaciation suggests a Southern Hemisphere “push” effect on the boreal summer EAM propagation.~~

~~The involvement of Southern Hemisphere “push” effects offers better interpretation on what have been responsible for the differences in the observed rate of changes of the EAM and Greenland interstadials and sub-interstadials and a much slower reorganization of the WPWP location or expansion/contraction with their impacts on atmosphere circulation are possibly attributed to the~~

~~differences too.~~

During the LGM ~~our~~the results indicate productivity minima that are consistent with previous observations in the NW Pacific, and severe vegetation/climate condition in the central Asia (Bezrukova et al., 2011). ~~and~~Therefore, strong regional sea ice covering ~~are~~is consistent with the hypothesis that ~~proposes~~ a strong stratification prevented ~~nutrients~~the supply of nutrients required for supporting productivity in surface waters (Gebhardt et al., 2008). The productivity proxies associated with calcareous phytoplankton productions show ~~significant~~ increased trends ~~since~~from 17.8 to 15.5 ka. These trends share the same structure ~~and~~the rate of changes ~~of~~with the gradual Antarctic warming accompanied by significantly diminished AMOC (McManus et al., 2004). The cooling of the N Atlantic surface water reduced water evaporation in the N Atlantic, as well as ~~and~~ Atlantic–Pacific moisture transport, ~~which~~This, in turn, facilitates the increased surface water salinity and decreases surface stratification in the N Pacific. The weakening stratification further intensifies the intermediate water ventilation in the N Pacific and ~~nutrients~~the supply of nutrients into the euphotic layer. ~~It is~~Especially noted~~eed~~is that a sharp increase of NW Pacific primary production since ~~nearly~~around 15.53 ka was indicated by nearly all productivity proxies, accompanied by some climate warming and decrease in sea ice covering. Subsequently, a strong productivity spike of sub-interstadial GI-1e at beginning of the B/A warming is associated with a resumption of the AMOC and the further decrease of sea ice influence, accompanied by rise ~~in~~of diatom production.

The synchronicity in changes of the NW Pacific centennial-millennial productivity events with the sub-interstadials in $\delta^{18}\text{O}$ of Chinese stalagmites calcite, Greenland ice cores and with the nuclide ^{14}C production during the EH (Figs. 4; ~~and~~ 5) imply that variability of the NW Pacific climate is tightly-strongly linked to summer EAM and N Atlantic/Greenland climate changes. The linkage is likely driven effectively by atmospheric coupling mechanisms forced by variations in solar irradiance variability. Regardless what specific driving mechanisms are responsible for the-

~~linkage teleconnection, strong causal linkages of~~ the centennial-millennial ~~productivity/climate and~~ ~~sub-stadial/interstadial productivity~~-variability in the NW Pacific ~~with sub-interstadials of summer~~ ~~and the linkage to~~-EAM from the LGM to EH reported here is a persistent feature of the high resolution far NW Pacific paleoceanography and sediment stratigraphy, ~~and is almost~~ synchronous with the Greenland/N Atlantic short-term changes.

Acknowledgements

~~We are grateful to Drs. Ralf Tiedemann and Dirk Nürnberg (AWI, GEOMAR, Germany) for a long and fruitful cooperation, and for providing samples and the dataset of core 12KL. We are indebted to Dr. John Southon (USA) for the AMS ¹⁴C dating.~~

This research work was supported by the RFBR—(Russia Fund of Basic Research)— Russia project (13-05-00296a, 16-55-53048 and 16-05-00127), Russian Federation budget No 01201363042, National Natural Science Foundation of China projects (41420104005, 40710069004 and 40431002) and the Russia-Taiwan Research Cooperation project 14-HHC-002 ~~and 17-MHT-003. We are appreciated to Dr. John Southon (USA) for AMS ¹⁴C dating.~~

References

~~Berger, W. H., Smetacek, V. S. and Wefer, G.: Ocean Productivity and Paleoproductivity - An Overview, in Productivity of the Ocean: Present and Past, pp. 1–34., 1989.~~

Bezrukova, E. V., Tarasov, P. E., Kulagina, N. V., Abzaeva, A. A., Letunova, P. P. and Kostrova, S. S.: Palynological study of Lake Kotokel' bottom sediments (Lake Baikal region), Russ. Geol. Geophys., 52(4), 458–465, doi:10.1016/j.rgg.2011.03.008, 2011.

Björck, S., Walker, M. J. C., Cwynar, L. C., Johnsen, S., Knudsen, K.-L., Lowe, J. J. and Wohlfarth, B.: An event stratigraphy for the Last Termination in the North Atlantic region based on the Greenland ice-core record: a proposal by the INTIMATE group, *J. Quat. Sci.*, 13(4), 283–292, doi:10.1002/(SICI)1099-1417(199807/08)13:4<283::AID-JQS386>3.0.CO;2-A, 1998.

[Bond, G. C., Kromer, B., Beer, J., Muscheler, R., Evans, M. N., Showers, W., Hoffmann, S., Lotti-Bond, R., Hajdas, I. and Bonani, G.: Persistent solar influence on North Atlantic climate during the Holocene., *Science*, 294\(5549\), 2130–6, doi:10.1126/science.1065680, 2001.](#)

Broecker, W. S.: Paleocean circulation during the Last Deglaciation: A bipolar seesaw?, *Paleoceanography*, 13(2), 119–121, doi:10.1029/97PA03707, 1998.

Caissie, B. E., Brigham-Grette, J., Lawrence, K. T., Herbert, T. D. and Cook, M. S.: Last Glacial Maximum to Holocene sea surface conditions at Umnak Plateau, Bering Sea, as inferred from diatom, alkenone, and stable isotope records, *Paleoceanography*, 25(1), PA1206, doi:10.1029/2008PA001671, 2010.

[Channell, J. E. T., Xuan, C. and Hodell, D. A.: Stacking paleointensity and oxygen isotope data for the last 1.5 Myr \(PISO-1500\), *Earth Planet. Sci. Lett.*, 283\(1–4\), 14–23, doi:10.1016/j.epsl.2009.03.012, 2009.](#)

Chikamoto, M. O., Menviel, L., Abe-Ouchi, A., Ohgaito, R., Timmermann, A., Okazaki, Y., Harada, N., Oka, A. and Mouchet, A.: Variability in North Pacific intermediate and deep water ventilation during Heinrich events in two coupled climate models, *Deep Sea Res. Part II Top. Stud. Oceanogr.*, 61–64, 114–126, doi:10.1016/j.dsr2.2011.12.002, 2012.

Dykoski, C. A., Edwards, R. L., Cheng, H., Yuan, D., Cai, Y., Zhang, M., Lin, Y., Qing, J., An, Z. and Revenaugh, J.: A high-resolution, absolute-dated Holocene and deglacial Asian monsoon record from Dongge Cave, China, *Earth Planet. Sci. Lett.*, 233(1–2), 71–86, doi:10.1016/j.epsl.2005.01.036, 2005.

[Dymond, J., Suess, E. and Lyle, M.: Barium in Deep-Sea Sediment: A Geochemical Proxy for Paleoproductivity, *Paleoceanography*, 7\(2\), 163–181, doi:10.1029/92PA00181, 1992.](#)

Enkin, R. J., Baker, J., Nourgaliev, D., Iassonov, P. and Hamilton, T. S.: Magnetic hysteresis parameters and Day plot analysis to characterize diagenetic alteration in gas hydrate-bearing sediments, *J. Geophys. Res.*, 112(B06S90), 1–13, doi:10.1029/2006JB004638, 2007.

EPICA Community Members: One-to-one coupling of glacial climate variability in Greenland and Antarctica, *Nature*, 444(7116), 195–198, doi:10.1038/nature05301, 2006.

Favorite, F., Dodimead, A. J. and Nasu, K.: Oceanography of the Subarctic Pacific region, 1960-1971., 1976.

Galbraith, E. D., Jaccard, S. L., Pedersen, T. F., Sigman, D. M., Haug, G. H., Cook, M., Southon, J. R. and Francois, R.: Carbon dioxide release from the North Pacific abyss during the last deglaciation., *Nature*, 449(7164), 890–893, doi:10.1038/nature06227, 2007.

[Ganopolski, A. and Rahmstorf, S.: Abrupt Glacial Climate Changes due to Stochastic Resonance, *Phys. Rev. Lett.*, 88\(3\), 38501, doi:10.1103/PhysRevLett.88.038501, 2002.](#)

Gebhardt, H., Sarnthein, M., Grootes, P. M., Kiefer, T., Kuehn, H., Schmieder, F. and Röhl, U.: Paleonutrient and productivity records from the subarctic North Pacific for Pleistocene glacial terminations I to V, *Paleoceanography*, 23(4), doi:10.1029/2007PA001513, 2008.

[Goldberg, E. D. and Arrhenius, G. O. S.: Chemistry of Pacific pelagic sediments, *Geochim. Cosmochim. Acta*, 13\(2–3\), 153–212, doi:10.1016/0016-7037\(58\)90046-2, 1958.](#)

Goldberg, E. L., Gorbarenko, S. A., Shaporenko, A. D., Bosin, A. A., Leskov, V. Y. and Chebykin, E. P.: Instability of last glacial climate from SRXFA data for bottom sediments in the Okhotsk Sea, *Nucl. Instruments Methods Phys. Res. Sect. A Accel. Spectrometers, Detect. Assoc. Equip.*, 543(1), 284–287, doi:10.1016/j.nima.2005.01.242, 2005.

Gorbarenko, S. A.: Stable Isotope and Lithologic Evidence of Late-Glacial and Holocene

Oceanography of the Northwestern Pacific and Its Marginal Seas, *Quat. Res.*, 46(3), 230–250, doi:10.1006/qres.1996.0063, 1996.

Gorbarenko, S. A. and Goldberg, E. L.: Assessment of Variations of Primary Production in the Sea of Okhotsk, Bering Sea, and Northwestern Pacific over the Last Glaciation Maximum and Holocene, *Dokl. Earth Sci.*, 405(9), 1380–1383, 2005.

Gorbarenko, S. A., Chekhovskaya, M. P. and Southon, J. R.: Detailed environmental changes of the Okhotsk Sea central part during last Glaciation Holocene, *Oceanologia*, 38(2), 305–308, 1998.

Gorbarenko, S. A., Leskov, V. Y., Artemova, A. V., Tiedemann, R., Biebow, N. and Nürnberg, D.: Ice Cover of the Sea of Okhotsk during the Last Glaciation and Holocene, *Dokl. Earth Sci.*, 389(2), 208–211, 2003.

Gorbarenko, S. A., Basov, I. A., Chekhovskaya, M. P. P., Southon, J. R., Khusid, T. A. A. and Artemova, A. V.: Orbital and millennium scale environmental changes in the southern Bering Sea during the last glacial-Holocene: Geochemical and paleontological evidence, *Deep Sea Res. Part II Top. Stud. Oceanogr.*, 52(16–18), 2174–2185, doi:10.1016/j.dsr2.2005.08.005, 2005.

[Gorbarenko, S. A., Harada, N., Malakhov, M. I., Velivetskaya, T. A., Vasilenko, Y. P., Bosin, A. A., Derkachev, A. N., Goldberg, E. L. and Ignatiev, A. V.: Responses of the Okhotsk Sea environment and sedimentology to global climate changes at the orbital and millennial scale during the last 350kyr, *Deep Sea Res. Part II Top. Stud. Oceanogr.*, 61–64, 73–84, doi:10.1016/j.dsr2.2011.05.016, 2012.](#)

Gorbarenko, S. A., Artemova, A. V., Goldberg, E. L. and Vasilenko, Y. P.: The response of the Okhotsk Sea environment to the orbital-millennium global climate changes during the Last Glacial Maximum, deglaciation and Holocene, *Glob. Planet. Change*, 116, 76–90, doi:10.1016/j.gloplacha.2014.02.002, 2014.

~~Harada, N.: JAMSTEC cruise report: RV Mirai cruise MR06-04-LEG1., 2006.~~

Harada, N.: MIRAI cruise report MR06-04 Leg 1 and 2, JAMSTEC, Yokosuka. [Available at http://www.godac.jamstec.go.jp/cruisedata/mirai/e/MR06-04_leg1.html], 2006.

Harris, P. G., Zhao, M., Rosell-Melé, A., Tiedemann, R., Sarnthein, M. and Maxwell, J. R.: Chlorin accumulation rate as a proxy for Quaternary marine primary productivity, *Nature*, 383(6595), 63–65, doi:10.1038/383063a0, 1996.

Hong, Y. T., Hong, B., Lin, Q. H., Shibata, Y., Zhu, Y. X., Leng, X. T. and Wang, Y.: Synchronous climate anomalies in the western North Pacific and North Atlantic regions during the last 14,000 years, *Quat. Sci. Rev.*, 28(9–10), 840–849, doi:10.1016/j.quascirev.2008.11.011, 2009.

Hu, F. S., Kaufman, D., Yoneji, S., Nelson, D., Shemesh, A., Huang, Y., Tian, J., Bond, G. C., Clegg, B. and Brown, T. A.: Cyclic variation and solar forcing of Holocene climate in the Alaskan subarctic., *Science*, 301(5641), 1890–1893, doi:10.1126/science.1088568, 2003.

Jaccard, S. L., Galbraith, E. D., Sigman, D. M. and Haug, G. H.: A pervasive link between Antarctic ice core and subarctic Pacific sediment records over the past 800kyrs, *Quat. Sci. Rev.*, 29(1–2), 206–212, doi:10.1016/j.quascirev.2009.10.007, 2010.

Jasonov, P. G., Nurgaliev, D. K., Burov, B. V. and Heller, F.: A modernized coercivity spectrometer, *Geol. Carpathica*, 49(3), 2254–225, 1998.

Johnsen, S. J., Clausen, H. B., Dansgaard, W., Fuhrer, K., Gundestrup, N., Hammer, C. U., Iversen, P., Jouzel, J., Stauffer, B. and Steffensen, J. P.: Irregular glacial interstadials recorded in a new Greenland ice core, *Nature*, 359(6393), 311–313, doi:10.1038/359311a0, 1992.

Keigwin, L. D.: Glacial-age hydrography of the far northwest Pacific Ocean, *Paleoceanography*, 13(4), 323–339, doi:10.1029/98PA00874, 1998.

Kiefer, T., Sarnthein, M., Erlenkeuser, H., Grootes, P. M. and Roberts, A. P.: North Pacific response to millennial-scale changes in ocean circulation over the last 60 kyr, *Paleoceanography*,

[16\(2\), 179–189, doi:10.1029/2000PA000545, 2001.](#)

Kienast, S. S. and McKay, J. L.: Sea surface temperature in the subarctic Northeast Pacific reflect millennial-scale climate oscillations during the last 16 kyr, *Geophys. Res. Lett.*, 28(8), 1563–1566, 2001.

Kuehn, H., Lembke-Jene, L., Gersonde, R., Esper, O., Lamy, F., Arz, H. W., Kuhn, G. and Tiedemann, R.: Laminated sediments in the Bering Sea reveal atmospheric teleconnections to Greenland climate on millennial to decadal timescales during the last deglaciation, *Clim. Past*, 10(6), 2215–2236, doi:10.5194/cp-10-2215-2014, 2014.

Lisitzin, A. P.: *Sea-Ice and Iceberg Sedimentation in the Ocean*, Springer, Berlin, Heidelberg., 2002.

Malakhov, M. I., Gorbarenko, S. A., Malakhova, G. Y., Harada, N., Vasilenko, Y. P., Bosin, A. A., Goldberg, E. L. and Derkachev, A. N.: Petromagnetic parameters of bottom sediments as indicators of the climatic and environmental changes in the central zone of the Sea of Okhotsk during the last 350 kyr, *Russ. Geol. Geophys.*, 50(11), 973–982, doi:10.1016/j.rgg.2009.10.006, 2009.

Max, L., Riethdorf, J.-R., Tiedemann, R., Smirnova, M., Lembke-Jene, L., Fahl, K., Nürnberg, D., Matul, A. G. and Mollenhauer, G.: Sea surface temperature variability and sea-ice extent in the subarctic northwest Pacific during the past 15,000 years, *Paleoceanography*, 27(3), doi:10.1029/2012PA002292, 2012.

Max, L., Lembke-Jene, L., Riethdorf, J.-R., Tiedemann, R., Nürnberg, D., Kühn, H. and Mackensen, A.: Pulses of enhanced North Pacific Intermediate Water ventilation from the Okhotsk Sea and Bering Sea during the last deglaciation, *Clim. Past*, 10(2), 591–605, doi:10.5194/cp-10-591-2014, 2014.

[McManus, J. F., Anderson, R. F., Broecker, W. S., Fleisher, M. Q. and Higgins, S. M.:](#)

[Radiometrically determined sedimentary fluxes in the sub-polar North Atlantic during the last 140,000 years, Earth Planet. Sci. Lett., 155\(1–2\), 29–43, doi:10.1016/S0012-821X\(97\)00201-X, 1998.](#)

McManus, J. F., Francois, R., Gherardi, J.-M., Keigwin, L. D. and Brown-Leger, S.: Collapse and rapid resumption of Atlantic meridional circulation linked to deglacial climate changes., *Nature*, 428(6985), 834–837, doi:10.1038/nature02494, 2004.

Nagashima, K., Tada, R., Tani, A., Sun, Y., Isozaki, Y., Toyoda, S. and Hasegawa, H.: Millennial-scale oscillations of the westerly jet path during the last glacial period, *J. Asian Earth Sci.*, 40(6), 1214–1220, doi:10.1016/j.jseas.2010.08.010, 2011.

[Narita, H., Sato, M., Tsunogai, S., Murayama, M., Ikehara, M., Nakatsuka, T., Wakatsuchi, M., Harada, N. and Ujiie, Y.: Biogenic opal indicating less productive northwestern North Pacific during the glacial ages, Geophys. Res. Lett., 29\(15\), 22-1-22-4, doi:10.1029/2001GL014320, 2002.](#)

North Greenland Ice Core Project members: High-resolution record of Northern Hemisphere climate extending into the last interglacial period, *Nature*, 431(7005), 147–151, doi:10.1038/nature02805, 2004.

Nürnberg, D. and Tiedemann, R.: Environmental change in the Sea of Okhotsk during the last 1.1 million years, *Paleoceanography*, 19(4), PA4011, doi:10.1029/2004PA001023, 2004.

Okazaki, Y., Timmermann, A., Menviel, L., Harada, N., Abe-Ouchi, A., Chikamoto, M. O., Mouchet, A. and Asahi, H.: Deepwater formation in the North Pacific during the Last Glacial Termination., *Science*, 329(5988), 200–204, doi:10.1126/science.1190612, 2010.

Praetorius, S. K. and Mix, A. C.: Synchronization of North Pacific and Greenland climates preceded abrupt deglacial warming, *Science*, 345(6195), 444–448, doi:10.1126/science.1252000, 2014.

[Prahl, F. G., Muehlhausen, L. A. and Lyle, M.: An organic geochemical assessment of](#)

[oceanographic conditions at Manop Site C over the past 26,000 years, *Paleoceanography*, 4\(5\), 495–510, doi:10.1029/PA004i005p00495, 1989.](#)

Rasmussen, S. O., Bigler, M., Blockley, S. P., Blunier, T., Buchardt, S. L., Clausen, H. B., Cvijanovic, I., Dahl-Jensen, D., Johnsen, S. J., Fischer, H., Gkinis, V., Guillevic, M., Hoek, W. Z., Lowe, J. J., Pedro, J. B., Popp, T., Seierstad, I. K., Steffensen, J. P., Svensson, A. M., Vallelonga, P., Vinther, B. M., Walker, M. J. C., Wheatley, J. J. and Winstrup, M.: A stratigraphic framework for abrupt climatic changes during the Last Glacial period based on three synchronized Greenland ice-core records: refining and extending the INTIMATE event stratigraphy, *Quat. Sci. Rev.*, 106, 14–28, doi:10.1016/j.quascirev.2014.09.007, 2014.

Reimer, P. J., Baillie, M. G. L., Bard, E., Beck, J. W., Bertrand, C. J. H., Blackwell, P. G., Buck, C. E., Burr, G. S., Cutler, K. B., Damon, P. E., Edwards, R. L., Fairbanks, R. G., Friedrich, M. and Guilderson, T. P.: IntCal04 terrestrial radiocarbon age calibration, 0–26 cal kyr BP, *Radiocarbon*, 46(3), 1029–1058, 2004.

~~Reimer, P. J., Baillie, M. G. L., Bard, E., Bayliss, A., Beck, J. W., Blackwell, P. G., Bronk-Ramsey, C., Buck, C. E., Burr, G. S., Edwards, R. L., Friedrich, M., Grootes, P. M., Guilderson, T. P., Hajdas, I., Heaton, T. J., Hogg, A. G., Hughen, K. A., Kaiser, K. F., Kromer, B., McCormac, F. G., Manning, S. W., Reimer, R. W., Richards, D. A., Southon, J. R., Talamo, S., Turney, C. S. M., Van Der Plicht, J. and Weyhenmeyer, C. E.: IntCal09 and Marine09 radiocarbon age calibration curves, 0–50,000 years cal BP, *Radiocarbon*, 51(4), 1111–1150, doi:10.2458/re.v51i4.3569, 2009.~~

[Reimer, P. J., Bard, E., Bayliss, A., Beck, J. W., Blackwell, P. G., Bronk Ramsey, C., Buck, C. E., Cheng, H., Edwards, R. L., Friedrich, M., Grootes, P. M., Guilderson, T. P., Haflidason, H., Hajdas, I., Hatte, C., Heaton, T. J., Hoffmann, D. L., Hogg, A. G., Hughen, K. A., Kaiser, K. F., Kromer, B., Manning, S. W., Niu, M., Reimer, R. W., Richards, D. A., Scott, E. M., Southon, J. R., Staff, R. A., Turney, C. S. M. and van der Plicht, J.: IntCal13 and Marine13 Radiocarbon Age](#)

[Calibration Curves 0–50,000 Years cal BP, Radiocarbon, 55\(4\), 1869–1887,](#)

[doi:10.2458/azu_js_rc.55.16947, 2013.](#)

Riethdorf, J.-R., Nürnberg, D., Max, L., Tiedemann, R., Gorbarenko, S. A. and Malakhov, M. I.: Millennial-scale variability of marine productivity and terrigenous matter supply in the western Bering Sea over the past 180 kyr, *Clim. Past*, 9(3), 1345–1373, doi:10.5194/cp-9-1345-2013, 2013.

[Riethdorf, J.-R., Thibodeau, B., Ikehara, M., Nürnberg, D., Max, L., Tiedemann, R. and Yokoyama, Y.: Surface nitrate utilization in the Bering sea since 180kA BP: Insight from sedimentary nitrogen isotopes, Deep Sea Res. Part II Top. Stud. Oceanogr., 125–126, 163–176, doi:10.1016/j.dsr2.2015.03.007, 2016.](#)

Röhl, U. and Abrams, L. J.: High-resolution, downhole, and nondestructive core measurements from Sites 999 and 1001 in the Caribbean Sea: application to the Late Paleocene Thermal Maximum, in *Proceedings of the Ocean Drilling Program, 165 Scientific Results*, vol. 165, pp. 191–203, Ocean Drilling Program., 2000.

Rohling, E. J., Liu, Q. S., Roberts, a. P., Stanford, J. D., Rasmussen, S. O., Langen, P. L. and Siddall, M.: Controls on the East Asian monsoon during the last glacial cycle, based on comparison between Hulu Cave and polar ice-core records, *Quat. Sci. Rev.*, 28, 3291–3302, doi:10.1016/j.quascirev.2009.09.007, 2009.

Rosignol-Strick, M.: Mediterranean Quaternary sapropels, an immediate response of the African monsoon to variation of insolation, *Palaeogeogr. Palaeoclimatol. Palaeoecol.*, 49(3–4), 237–263, doi:10.1016/0031-0182(85)90056-2, 1985.

[Rothwell, R. G.: The Smear Slide Method, in Minerals and Mineraloids in Marine Sediments, pp. 21–24, Springer Netherlands, Dordrecht., 1989.](#)

[Ruth, U., Bigler, M., Röthlisberger, R., Siggaard-Andersen, M.-L., Kipfstuhl, S.,](#)

Goto-Azuma, K., Hansson, M. E., Johnsen, S. J., Lu, H. and Steffensen, J. P.: Ice core evidence for a very tight link between North Atlantic and east Asian glacial climate, *Geophys. Res. Lett.*, 34(L03706), 1–5, doi:10.1029/2006GL027876, 2007.

Saenko, O. A., Schmittner, A. and Weaver, A. J.: The Atlantic–Pacific Seesaw, *J. Clim.*, 17(11), 2033–2038, doi:10.1175/1520-0442(2004)017<2033:TAS>2.0.CO;2, 2004.

Sakamoto, T., Ikehara, M., Aoki, K., Iijima, K., Kimura, N., Nakatsuka, T. and Wakatsuchi, M.: Ice-rafted debris (IRD)-based sea-ice expansion events during the past 100kyrs in the Okhotsk Sea, *Deep Sea Res. Part II Top. Stud. Oceanogr.*, 52(16–18), 2275–2301, doi:10.1016/j.dsr2.2005.08.007, 2005.

Sarnthein, M., Kiefer, T., Grootes, P. M., Elderfield, H. and Erlenkeuser, H.: Warmings in the far northwestern Pacific promoted pre-Clovis immigration to America during Heinrich event 1, *Geology*, 34(3), 141–144, doi:10.1130/G22200.1, 2006.

Schlung, S. A., Christina Ravelo, A., Aiello, I. W., Andreasen, D. H., Cook, M. S., Drake, M., Dyez, K. A., Guilderson, T. P., LaRiviere, J. P., Stroynowski, Z. and Takahashi, K.: Millennial-scale climate change and intermediate water circulation in the Bering Sea from 90 ka: A high-resolution record from IODP Site U1340, *Paleoceanography*, 28(1), 54–67, doi:10.1029/2012PA002365, 2013.

Seierstad, I. K., Abbott, P. M., Bigler, M., Blunier, T., Bourne, A. J., Brook, E. J., Buchardt, S. L., Buizert, C., Clausen, H. B., Cook, E., Dahl-Jensen, D., Davies, S. M., Guillevic, M., Johnsen, S. J., Pedersen, D. S., Popp, T. J., Rasmussen, S. O., Severinghaus, J. P., Svensson, A. and Vinther, B. M.: Consistently dated records from the Greenland GRIP, GISP2 and NGRIP ice cores for the past 104 ka reveal regional millennial-scale $\delta^{18}\text{O}$ gradients with possible Heinrich event imprint, *Quat. Sci. Rev.*, 106, 29–46, doi:10.1016/j.quascirev.2014.10.032, 2014.

Seki, O., Ishiwatari, R. and Matsumoto, K.: Millennial climate oscillations in NE Pacific

surface waters over the last 82 kyr: New evidence from alkenones, *Geophys. Res. Lett.*, 29(23), 59-1-59-4, doi:10.1029/2002GL015200, 2002.

Seki, O., Ikehara, M., Kawamura, K., Nakatsuka, T., Ohnishi, K., Wakatsuchi, M., Narita, H. and Sakamoto, T.: Reconstruction of paleoproductivity in the Sea of Okhotsk over the last 30 kyr, *Paleoceanography*, 19(1), doi:10.1029/2002PA000808, 2004.

Serno, S., Winckler, G., Anderson, R. F., Maier, E., Ren, H., Gersonde, R. and Haug, G. H.: Comparing dust flux records from the Subarctic North Pacific and Greenland: Implications for atmospheric transport to Greenland and for the application of dust as a chronostratigraphic tool, *Paleoceanography*, 30(6), 583–600, doi:10.1002/2014PA002748, 2015.

Steffensen, J. P., Andersen, K. K., Bigler, M., Clausen, H. B., Dahl-Jensen, D., Fischer, H., Goto-Azuma, K., Hansson, M. E., Johnsen, S. J., Jouzel, J., Masson-Delmotte, V., Popp, T., Rasmussen, S. O., Röthlisberger, R., Ruth, U., Stauffer, B., Siggaard-Andersen, M.-L., Sveinbjörnsdóttir, A. E., Svensson, A. M. and White, J. W. C.: High-resolution Greenland ice core data show abrupt climate change happens in few years., *Science*, 321(5889), 680–684, doi:10.1126/science.1157707, 2008.

Stuiver, M. and Reimer, P. J.: Extended 14C Data Base and Revised Calib 3.0 14C Age Calibration Program, *Radiocarbon*, 35(1), 215–230, 1993.

Sun, Y., Clemens, S. C., Morrill, C., Lin, X., Wang, X. and An, Z.: Influence of Atlantic meridional overturning circulation on the East Asian winter monsoon, *Nat. Geosci.*, 5(1), 46–49, doi:10.1038/ngeo1326, 2011.

Tauxe, L.: Sedimentary records of relative paleointensity of the geomagnetic field: Theory and practice, *Rev. Geophys.*, 31(3), 319, doi:10.1029/93RG01771, 1993.

Walker, M. J. C., Berkelhammer, M., Björck, S., Cwynar, L. C., Fisher, D. A., Long, A. J., Lowe, J. J., Newnham, R. M., Rasmussen, S. O. and Weiss, H.: Formal subdivision of the Holocene Series/Epoch: a Discussion Paper by a Working Group of INTIMATE (Integration of ice-core,

marine and terrestrial records) and the Subcommittee on Quaternary Stratigraphy (International Commission on Stratigraphy), *J. Quat. Sci.*, 27(7), 649–659, doi:10.1002/jqs.2565, 2012.

Wang, Y., Cheng, H., Edwards, R. L., An, Z., Wu, J., Shen, C.-C. and Dorale, J. A.: A high-resolution absolute-dated late Pleistocene Monsoon record from Hulu Cave, China., *Science*, 294(5550), 2345–8, doi:10.1126/science.1064618, 2001.

Wang, Y., Cheng, H., Edwards, R. L., He, Y., Kong, X., An, Z., Wu, J., Kelly, M. J., Dykoski, C. A. and Li, X.: The Holocene Asian monsoon: links to solar changes and North Atlantic climate., *Science*, 308(5723), 854–857, doi:10.1126/science.1106296, 2005.

Wang, Y., Cheng, H., Edwards, R. L., Kong, X., Shao, X., Chen, S., Wu, J., Jiang, X., Wang, X. and An, Z.: Millennial- and orbital-scale changes in the East Asian monsoon over the past 224,000 years., *Nature*, 451(7182), 1090–1093, doi:10.1038/nature06692, 2008.

[Wu, B. and Wang, J.: Winter Arctic Oscillation, Siberian High and East Asian Winter Monsoon, *Geophys. Res. Lett.*, 29\(19\), 3-1-3-4, doi:10.1029/2002GL015373, 2002.](#)

Xue, F., Wang, H. and He, J.: Interannual Variability of Mascarene High and Australian High and Their Influences on East Asian Summer Monsoon, *J. Meteorol. Soc. Japan*, 82(4), 1173–1186, doi:10.2151/jmsj.2004.1173, 2004.

Yu, J., Anderson, R. F., Jin, Z., Menviel, L., Zhang, F., Ryerson, F. J. and Rohling, E. J.: Deep South Atlantic carbonate chemistry and increased interocean deep water exchange during last deglaciation, *Quat. Sci. Rev.*, 90, 80–89, doi:10.1016/j.quascirev.2014.02.018, 2014.

Yu, Y., Yang, T., Li, J., Liu, J., An, C., Liu, X., Fan, Z., Lu, Z., Li, Y. and Su, X.: Millennial-scale Holocene climate variability in the NW China drylands and links to the tropical Pacific and the North Atlantic, *Palaeogeogr. Palaeoclimatol. Palaeoecol.*, 233(1–2), 149–162, doi:10.1016/j.palaeo.2005.09.008, 2006.

Yuan, D., Cheng, H., Edwards, R. L., Dykoski, C. A., Kelly, M. J., Zhang, M., Qing, J., Lin,

Y., Wang, Y., Wu, J., Dorale, J. A., An, Z. and Cai, Y.: Timing, duration, and transitions of the last interglacial Asian monsoon., *Science*, 304(5670), 575–578, doi:10.1126/science.1091220, 2004.

Zakharkov, S. P., Gorbarenko, S. A. and Bosin, A. A.: Chlorin content in sea sediments as an indication of sea primary productivity (in Russian), *Bull. Far East. Branch Russ. Acad. Sci.*, 1, 52–58, 2007.

Zijderveld, J. D. A.: A. C. demagnetization of rocks : analysis of results, in *Methods in Palaeomagnetism*, edited by D. W. Collinson, K. M. Creer, and S. K. Runcorn, pp. 254–286, Elsevier., 1964.

Table 1. AMS ¹⁴C data on monospecies planktonic foraminifera *N. pachyderma* sin. and benthic foraminifera *Epistominella pacifica* and *Uvigerina parvocastata* of core 41-2. All measured ¹⁴C age data were corrected by NW Pacific surface water reservoir ages of 900 years (Max et al., 2012). In case of using benthic foraminifera ~~for dating~~ we accept difference in coeval benthic-planktic foraminifera ages equals to 1400 years for depth water ~~1900~~1940 m, based on the unpublished datum and ~~total-regional~~ results of Max et al. (2014). All radiocarbon ages were converted into calibrated 1-sigma calendar age using the calibration program CALIB REV 7.0.1 (Stuiver and Reimer, 1993) with the Marine13 calibration curve (Reimer et al., 2013).

#	Lab. code	core depth cm	foraminifera species	¹⁴ C-age year	Err.1 sigma year	calendar- age, years	calendar age, ka
1	YAUT-021713	120	<i>E. pacifica</i>	10078	47	9121-	9.121
2	YAUT-021714	127.5	<i>E. pacifica</i>	10340	42	9445-	9.445

3	UCIAMS-148095	298	<i>N. pachyd.</i>	13160	50	14393	14.393
4	UCIAMS-148096	156	<i>Uv. parvoc.</i>	11135	45	10600	10.60
5	UCIAMS-148098	306	<i>Uv. parvoc.</i>	14185	35	16,016	14.616

Table 2. Centennial-millennial productivity increase/environment amelioration events over 25-8 ka ago plus abrupt productivity drop/cooling Events during Early Holocene in the NW Pacific core 41-2 which had occurred in-phase with Chinese sub interstadials (CsI) of the summer EAM intensification and Chinese sub stadials (CsS) of winter EAM activation.

<u>Events</u>	<u>Core interval, cm</u>	<u>Averaged cal. age, ka</u>
<u>CsS-EH-1</u>	<u>106-110</u>	<u>8.2</u>
<u>CsS-EH-2</u>	<u>117-123</u>	<u>9.2</u>
<u>CsI-EH-1</u>	<u>125-132</u>	<u>9.8</u>
<u>CsS-EH-3</u>	<u>138-143</u>	<u>10.2</u>
<u>CsI-EH-2</u>	<u>148-153</u>	<u>10.7</u>
<u>CsS-EH-4</u>	<u>155-159</u>	<u>10.95</u>
<u>CsS-EH-4'</u>	<u>162-167</u>	<u>11.15</u>
<u>CsI-EH-3</u>	<u>168-181</u>	<u>11.4</u>
<u>CsI-GI1-a</u>	<u>233-243</u>	<u>13.05</u>
<u>CsI-GI1-c1</u>	<u>248-262</u>	<u>13.5</u>
<u>CsI-GI1-c3</u>	<u>268-278</u>	<u>13.8</u>
<u>CsI-GI1-e</u>	<u>291-312</u>	<u>14.45</u>
<u>CsI-GS2.1-1</u>	<u>335-340</u>	<u>15.45</u>
<u>CsI-GS2.1-2</u>	<u>355-362</u>	<u>16.55</u>
<u>CsI-GS2.1-3</u>	<u>375-383</u>	<u>17.56</u>
<u>CsI-GS2.1-4</u>	<u>388-395</u>	<u>18.1</u>
<u>CsI-GS2.1-5</u>	<u>400-410</u>	<u>18.85</u>
<u>CsI-GS2.1-6</u>	<u>431-447</u>	<u>19.8</u>

Table ~~32~~. The key time points of core 41-2 based on the available AMS ¹⁴C data of core

41-2, ~~depths correlated with projection of~~ AMS ¹⁴C data of core 12KL on the core 41-2 depth
according to correlation of related increased productivity events and RPI records plus ~~depth-~~
correlation of the productivity ~~eyeles events~~ with related sub-interstadials of the highly resolved,
absolutely dated E Asia monsoon ~~related CsIs~~ (Wang et al., 2008) beyond the projected ¹⁴C data.
AMS ¹⁴C datum of core 12KL and age at depth of 706 cm was accepted according to the
Tiedemann/Max age model 2 (Max et al., 2012, 2014).

Depth	AMS 14C core	AMS 14C data (ka)/ <u>Key</u>	<u>correlation with ages of</u>	<u>Accepted key</u>
	41-2	<u>time points of core 12KL</u>	<u>China subInterstadial</u>	<u>time points</u>
cm	(cal. kyr BP)	depth of core 12KL, cm	<u>Age, ka/CsI ages of</u>	<u>calendar age</u>
	<u>Cal. age, ka</u>	<u>ka/ depth (cm)</u>	China sub-Interstadial	<u>Cal. age, ka</u>
120	9.12			9.12
127.5	9.45			
126		9.51/210		9.51
156	10.6			
159		11.08/295		11.08
167		11.31/340		11.31
<u>239</u>			<u>13.0/CsI-GI1-a</u>	<u>13.0</u>
251		13. 4238 /508		13. 4238
273		13.79/550		13.79
298	14.39			
303		14.42/611		14.42
306	14.61			

337		15.42/ <u>CsI-GS2.1-1</u>	15.42
347-348	15.9(15.55)/695		16.16
	<u>16.16/706</u>		
357		16.51/ <u>CsI-GS2.1-2</u>	16.51
382-379		17.56/ <u>CsI-GS2.1-3</u>	17.56
393		18.12/ <u>CsI-GS2.1-4</u>	18.12
402	18.6/821		<u>18.6</u>
405		18.8	18.8
431	19.54/876		
438		19.8	19.8

Figures

Fig. 1. Bathymetry, surface water currents and location of the cores 41-2 (star) and 12KL (cross) (Max et al., 2012) in the North Pacific. Surface currents as in (Favorite et al., 1976) with modifications. EKC – East Kamchatka Current, WKC – West Kamchatka Current.

Fig. 2. Records (from bottom to top) of the ~~weight percentages of the CF~~, share of volcanic grains in the sediment fraction ~~more~~ $\geq 150 \mu\text{m}$, weight percentages of the CF, magnetic susceptibility (MS), paramagnetic magnetization (PM), color b^* ; TOC, Chlorin, CaCO_3 , Ba-bio, Si-bio (opal) and Br-bio content versus core 41-2 depth. Preliminary boundaries of B/A warming, YD cooling and Holocene are shown according to total regularities of productivity variability in the NW Pacific, the Sea of Okhotsk and Bering Sea (Galbraith et al., 2007; Gorbarenko, 1996; Gorbarenko and

Goldberg, 2005; Keigwin, 1998; Seki et al., 2004) and AMS ^{14}C data (calendar ka) shown at the base. Yellow (blue) bars depict the centennial-millennial increased productivity/environmental amelioration (cooling) events according to most productivity proxies and decreases in PM. Blue bars depict the centennial-millennial decreased productivity/environmental cooling events during EH.

Fig. 3. Correlation of the increased productivity event cycles in the cores 41-2 (low panel) and with those in 12KL (middle panel) versus depth with sub-interstadials of the $\delta^{18}\text{O}$ calcite of Chinese stalagmites (Dykoski et al., 2005; Wang et al., 2008) (upper panel) and key time points of core 41-2 shown by red lines.

Productivity cycles for cores 41-2 are based on the stack suite of productivity proxies and PM records (Fig. 2) and 12KL (Ca, chlorin, and color b^* and PM records) were correlated according to synchronously changes in productivity proxies, paramagnetic magnetization, magnetic relative paleomagnetic intensity (RPI) and ^{14}C AMS data of the both cores. AMS ^{14}C data of core 41-2 is shown at the base. According to the correlation of the productivity cycles and curves of RPI, the red lines are related to key time points with ^{14}C AMS data of core 12KL (middle panel) and the green lines with the relative Chinese sub-interstadials of the $\delta^{18}\text{O}$ calcite of Chinese stalagmites (Wang et al., 2008) (upper panel) were projected into corresponded depths of core 41-2 (bottom panel). Yellow (blue) bars depict the centennial-millennial increased productivity/environmental amelioration (cooling) events according to most productivity proxies and decreases in PM. Color b^* and Ca content, AMS ^{14}C data of core 12KL and its depth-age correlation with the Greenland NGRIP ice core were introduced from site <http://dx.doi.org/10.1594/PANGAEA.830222>. Blue lines correlate the productivity cycles of cores 41-2 and 12KL with relative Chinese sub-interstadials of the $\delta^{18}\text{O}$ calcite of Chinese stalagmites (Dykoski et al., 2005; Wang et al., 2008) during LGM-EH in consistence with their age models.

Fig. 4. High resolution variability of the productivity and lithologic proxies in the NW Pacific (off Kamchatka) over the 21-8 ka ~~ago~~-period. CF percentages, MS, paramagnetic magnetization and color b^* , chlorin, CaCO_3 , ~~TOC, Br-bio, Ba-bio and Si-bio (analog of biogenic opal)~~ content determined in cores 41-2 (blue lines) and 12KL (red lines) are shown from bottom to top. The NW Pacific centennial-millennial productivity cycles characterized by an increase in most productivity proxies are clearly associated with the abrupt summer EAM intensification revealed in the Chinese cave stalagmites, ~~called defined~~ as sub-~~l~~-interstadial, and less pronounced with short-~~term~~ events in the Greenland ice cores $\delta^{18}\text{O}$ records. Linear ~~lines-trends are shown~~ ~~trends of the siliceous and carbonaceous related~~ trends for the productivity indices over LGM and HE 1. Yellow (blue) bars depict the centennial-millennial increased productivity/environmental amelioration (cooling) events according to most productivity proxies and decreases in PM.

Fig. 5. Compilation on N-S hemisphere milestone climate records, solar activity, NW Pacific productivity cycles and Southern Siberia environment during the last 25 ka. From bottom to top: absolutely dated $\delta^{18}\text{O}$ calcite of Chinese cave stalagmites (Dykoski et al., 2005; Wang et al., 2008) characterized EAM activity; the residual atmospheric $\Delta^{14}\text{C}$ record of around 2000-year moving average (Reimer et al., 2004) indicated solar irradiance variability; oxygen isotope EDML records after methane synchronization with the North Greenland ice core (EPICA Community Members, 2006); the petrologic tracer of drift ice in the N Atlantic (Bond et al., 2001); the $\delta^{18}\text{O}$ and Ca^{2+} records in the Greenland NGRIP and GISP 2 ice core indicated air temperature and dust variability on GICC05 age scale (Rasmussen et al., 2014), ~~and~~ pollen reconstructed Southern Siberia environment changes (Lake Kotokel, Lake Baikal region) (Bezrukova et al., 2011); and productivity stack for core 41-2. The vertical yellow bands trace the centennial-millennial NW Pacific productivity cycles with increased productivity, blue bars GS/CS-3.1 (HE 2) and Early Holocene short term coolings. Yellow (blue) bars depict the centennial-millennial increased

productivity/environmental amelioration (cooling) events. NW Pacific centennial-millennial productivity cycles are accompanied by interstadial and sub-interstadial intensification of the summer EAM over 25-8 ka, ~~age~~ and increase of solar irradiance during B/A and EH short term warmings. Their correlation with short term increased Greenland temperature (NGRIP ice core) and a decreased Antarctic temperature are less pronounced but seem to be marked as well.

Fig. 6. Cross correlation of the EAM and Greenland climate variability calculated by correlation of $\delta^{18}\text{O}$ values of the calcite of Chinese stalagmites (Wang et al., 2008) with ~~ones-those~~ of the NGRIP (lower panel) and ~~with ones-of-the~~ GISP 2 (upper panel) ice cores (Rasmussen et al., 2014) by-using moving windows at 1000 years (purple lines), 2000 years (red lines) and 3000 years (green lines) over the last 25 ka. Yellow bars show areas with insignificant cross correlation ranging between +0.25 and -0.25. Cross correlation between the EAM and Greenland by-using a moving window 3000 years is negative during the period of 16.5-~~8.59-0~~ ka, and insignificant or weakly negative during earlier and later periods of 25-16.5 ka and of ~~9.08.5~~-0 ka ~~BP~~ confirmed the EAM and the Greenland synchronicity.